ELSEVIER

Contents lists available at ScienceDirect

# Construction and Building Materials

journal homepage: www.elsevier.com/locate/conbuildmat





# Highly thixotropic ultra-high-performance concrete (UHPC) as an overlay

Jiang Du, Pengwei Guo, Zhuo Liu, Weina Meng

Department of Civil, Environmental and Ocean Engineering, Stevens Institute of Technology, Hoboken, NJ 07030, USA

#### ARTICLE INFO

Keywords: ultra-high-performance concrete (UHPC) overlay Water-based nanoclay Thixotropy Vibration index Bond strength

#### ABSTRACT

Ultra-high-performance concrete (UHPC) is an emerging overlay material for the bridge deck rehabilitation. As a durable material, UHPC overlay can effectively extend the service life of the bridge. In this study, the highly thixotropic UHPC overlay was designed and developed to facilitate sloped overlay construction with minimum formworks. A new type of water-based and well-dispersed nanoclay suspension was utilized to enhance the thixotropy. Two indices, including initial fluctuation of yield stress ( $\tau_{floc}$ ) and thixotropy index ( $I_A$ ), were proposed to evaluate the thixotropy of fresh UHPC. It was found that, as nanoclay contents increased from 0 to 0.20 % (by mass of binders), the initial fluctuation of yield stress ( $\tau_{floc}$ ) increased from 392.7 Pa to 3290.1 Pa and the thixotropy index ( $I_A$ ) increased from 9.7 Pa/min to 16.4 Pa/min, representing the significant enhancement on thixotropy. The highly thixotropic UHPC overlay showed good shape stability after the placement, but showing plenty of defects on the interface. It was shown that the bond strengths between thixotropic UHPC overlay and substrate are reduced by over 30 %. To address this issue, the application of proper vibration index on highly thixotropic UHPC overlay was investigated. Results showed that the bond strength between thixotropic UHPC overlay and substrate was increased by 45 % after the optimal vibration index. The SEM observation of the interface confirmed the increased air voids for highly thixotropic UHPC overlay and the reduced air voids after optimal vibration index. This study will promote the acceptance of highly thixotropic UHPC as an overlay.

#### 1. Introduction

Ultra-high-performance concrete (UHPC) is an advanced class of cementitious composites that features superior mechanical performances, self-consolidating property, and excellent durability due to the extremely low water-to-binder ratio (w/b < 0.25) and high packing density [1-7]. UHPC has been widely used in highway bridge construction for precast girders and piles [8-11], cast-in-situ connections and joints [12–15], jackets for columns [16], and bridge deck overlays [17-22]. As an overlay material, UHPC provides better structural strength [23], abrasion resistance [24], bonding performance [25,26], and protection from chloride intrusion [27] compared with other types of overlay materials [28-30]. In addition, compared to conventional concrete, the dead load of UHPC overlay is significantly lower due to reduced thickness [17,31]. However, in order to effectively drain away the external water (e.g., raining or snowing), the bridge deck overlay is a type of sloped structure and the slope is usually ranged from 2 % to 5 %, even up to 15 % in some extreme cases. When the typical UHPC with highly flowable and low thixotropy are applied as overlay materials [19], UHPC can flow freely under gravity effect and be hard to stay still on the sloped structures. Therefore, a large amount of formworks is needed to shape the fresh UHPC on the sloped structure after the casting and placement, which increases the construction cost and prolongs the construction time [32].

Currently, the development of new types of UHPC with high thixotropy is a promising approach to enhance the shape stability of fresh UHPC on sloped structures, thus reducing the use of formworks for bridge deck overlay constructions [17,19,33]. Highly thixotropic fluid behaves as solid under static conditions and flows under agitation or vibration [34]. Even if the flowable status is needed in some cases, the proper external interventions (e.g., vibration and shearing) can be applied to transfer the stable fresh UHPC to flowable status [17]. In addition to addressing the sloped casting issues, the development of highly thixotropic UHPC is also vital for 3D printing [35–37], aggregate settlement [38], and fiber distribution [39,40].

The thixotropic property of cement-based materials can be effectively enhanced by adding viscosity-modifying agent (VMA) [41–43]. According to the chemical compositions, VMA can be divided into organic type and inorganic type [42]. The organic VMAs include diutan gum and welan gum [44,45]. The organic VMAs are mainly composed

E-mail address: wmeng3@stevens.edu (W. Meng).

<sup>\*</sup> Corresponding author.

**Table 1**Chemical and physical properties of raw materials.

Components	Type I cement	Slag	Nanoclay	River sand
SiO <sub>2</sub> (%)	22.44	36.21	55.20	80.30
Al <sub>2</sub> O <sub>3</sub> (%)	2.76	11.10	12.20	10.50
Fe <sub>2</sub> O <sub>3</sub> (%)	2.24	0.76	4.05	3.43
CaO (%)	68.05	43.75	1.98	1.72
MgO (%)	0.91	5.09	8.56	1.70
SO <sub>3</sub> (%)	2.25	2.21	_	1.07
Na <sub>2</sub> O (%)	0.19	0.23	0.53	_
K <sub>2</sub> O (%)	0.11	0.40	0.68	_
TiO <sub>2</sub> (%)	0.14	0.58	0.49	_
P <sub>2</sub> O <sub>5</sub> (%)	0.09	0.02	0.65	_
C <sub>3</sub> S (%)	62.35	-	_	-
C <sub>2</sub> S (%)	20.28	-	_	-
C <sub>3</sub> A (%)	1.42	_	_	_
C <sub>4</sub> AF (%)	5.83	-	-	_
Loss of ignition (%)	1.28	0.72	15.66	1.28
Specific gravity (g/cm <sup>3</sup> )	3.15	2.9	1.14	2.65

with polymer coils, which can interpenetrate and entangle to form networks with attractive interactions to increase the thixotropy [45]. For example, Ma et al. [45] investigated the effect of diutan gum on thixotropy of cement pastes with a w/b of 0.34. The results showed that as diutan gum content increased from 0 to 2.5 %, the thixotropy index (i. e., growth rate of static yield stress) was increased by 650 %. Teng et al. [44] studied the effect of welan gum on thixotropy of UHPC mortars with a w/b of 0.2. The results showed that as welan gum content increased from 0 to 0.09 %, the thixotropy index (i.e., growth rate of static yield stress in rest time over 30 min) was increased by 240 %, and the initial increase of the yield stress (i.e., difference between the initial static yield stress and dynamic yield stress) was increased by 135 %. On the other hand, the inorganic VMAs include bentonite and nanomaterials (e.g., nanosilica, nano-CaCO<sub>3</sub>, and nanoclay) [46-50]. Specifically, bentonite is a yellow-white flake clay with montmorillonite as the primary component, with minor presence of quartz and calcium carbonate. Due to the strong water swelling and PCE adsorption effect, the addition of bentonite can efficiently increase the thixotropy of UHPC. Li et al. [46] revealed that, as the bentonite content increased from 0 to 12.5 %, the thixotropy index (i.e., thixotropic area method) was increased by 30 %. In addition, nanomaterials can fill the gaps between cement particles and increase physical contact points (known as the physical packing effect), which in turn to increase the thixotropy [51]. Besides, the use of nanoparticles can promote the hydration reaction and improve thixotropy due to the seeding effect [44]. For instance, Yuan et al [52] studied the effect of nanosilica on thixotropy of cement pastes with a w/b of 0.3. The results showed that as nanosilica content increased from 0 to 2 %, the thixotropy (i.e., breakdown area) was increased by 60 %. Oian and Kawashima [53] studied the effect of dry nanoclay powders on thixotropy of cement pastes with a w/b of 0.36. The results showed that as the nanoclay content increased from 0 to 0.5 %, the thixotropy (i.e., growth rate of static yield stress) was increased by 190 %. In summary, the addition of VMA can effectively enhance the thixotropy of UHPC and the thixotropy regulation of UHPC mixture is of great importance for its promotions.

However, nanoclay is a more attractive candidate for UHPC overlay applications due to the following reasons: (1) Nanoclay has an immediate stiffening effect on fresh UHPC which instantly increases the static yield stress due to the particles flocculation effect [54]. (2) Nanoclay has good compatibility with polycarboxylate ether (PCE) type superplasticizer [49] because it only absorbs a small amount of HRWR, so that HRWR has negligible impact on the thixotropy of UHPC containing nanoclay. (3) Adding nanoclay efficiently promotes the hydration of cement-based materials, leading to a higher proportion of irreversible structure build-up, which benefits the shape stability of UHPC [45].

The most commonly used nanoclay is a type of needle-like dry powder, which is approximately 1.75  $\mu m$  in length and 30 nm in

diameter [47,49,51,53,55]. In this case, some special pretreatments (e. g., ultra-sonification technology and surfactant technology) are highly required to ensure the uniform dispersion of nanoclay before the UHPC mixing process. Otherwise, the poor dispersion of nanocaly can undermine the key properties of UHPC instead. [56]. For instance, Gdoutos et al. [57] proposed an ultra-sonification technology to undermine agglomeration and facilitate the uniform dispersion of nanomaterials in aqueous media. Peyvandi et al. [58] claimed surfactants converted hydrophobic surfaces of carbon nanomaterials into hydrophilic surfaces for better dispersion. However, these advanced technologies are not practical for the large-scale production on job sites, which limited the promotion of nanomaterials for cast-in-place infrastructure. In this research, a new type of water-based nanoclay suspension is utilized to enhance thixotropy of UHPC for the first time. It is still unknown whether this new type of nanoclay suspension can efficiently work in fresh UHPC and how this nanoclay suspension affect the key properties

Apart from the first applications of water-based nanoclay suspension in UHPC system, another concern is the negative effect of high thixotropy on the bond behaviors between newly-cast overlay and old substrate concrete. For example, Federal Highway Administration (FHWA) successfully applied a type of thixotropic UHPC mixture for bridge deck overlays [17,19], however, the direct bond strength of thixotropic UHPC overlay was decreased by more than 10 % at 14 days compared to that of non-thixotropic UHPC overlay [19]. Due to heavy traffic loadings, the interface between overlay and substrate is subjected to high and repetitive shear and flexural stress [59-61]. The reduction of bond strength, especially at early ages, may undermine the durability and shorten the service life of the structure [62–64]. It is urgent to reveal the underlying mechanisms that leads to the reduction of bond strength between overlay and substrate. Moreover, it is also necessary to provide the corresponding methods to improve bond strength when using UHPC with high thixotropy for bridge deck overlay construction [17,65].

In summary, some challenges concerning real-life constructions should be identified: (1) how does the thixotropic properties of UHPC overlay affect the bond strength of the interface? (2) how does the thixotropic UHPC overlay interact with roughened surface of the substrate concrete? (3) How to address the potential issues that the bond strength of interface is reduced due to the application of the highly thixotropic UHPC overlay?

To address the above-mentioned challenges, a new type of water-based and well-dispersed attapulgite nanoclay suspension is utilized to enhance the thixotropy of UHPC mixtures. This research has the following main objectives: (1) to study the effect and elaborate the mechanisms of water-based nanoclay suspension on the thixotropic properties of UHPC; (2) to investigate the effect and elaborate the mechanism of water-based nanoclay on other key properties of UHPC, including workability, buildability, mechanical strength, and autogenous shrinakge; (3) to understand the effect of thixotropic properties of UHPC on the interfacial properties; (5) to explore the effect of vibration index on the interfacial properties. This research can advance the fundamental knowledge of UHPC and facilitates the further application of UHPC as overlay for sloped structures.

#### 2. Materials and mixing procedures

# 2.1. Raw materials

Type I Portland cement and slag are from a local supplier in New Jersey, U.S., which were employed as binder materials. The water-based nanoclay suspension with a solid mass content of 19.5 %, a specific gravity of 1.14, and the pH value of 8.5 was used to adjust the thixotropic properties of UHPC. The river sand was the fine aggregate. The chemical compositions and physical characteristics of those raw materials are listed in Table 1.

In addition, the particle size distribution curves of the Type I cement,

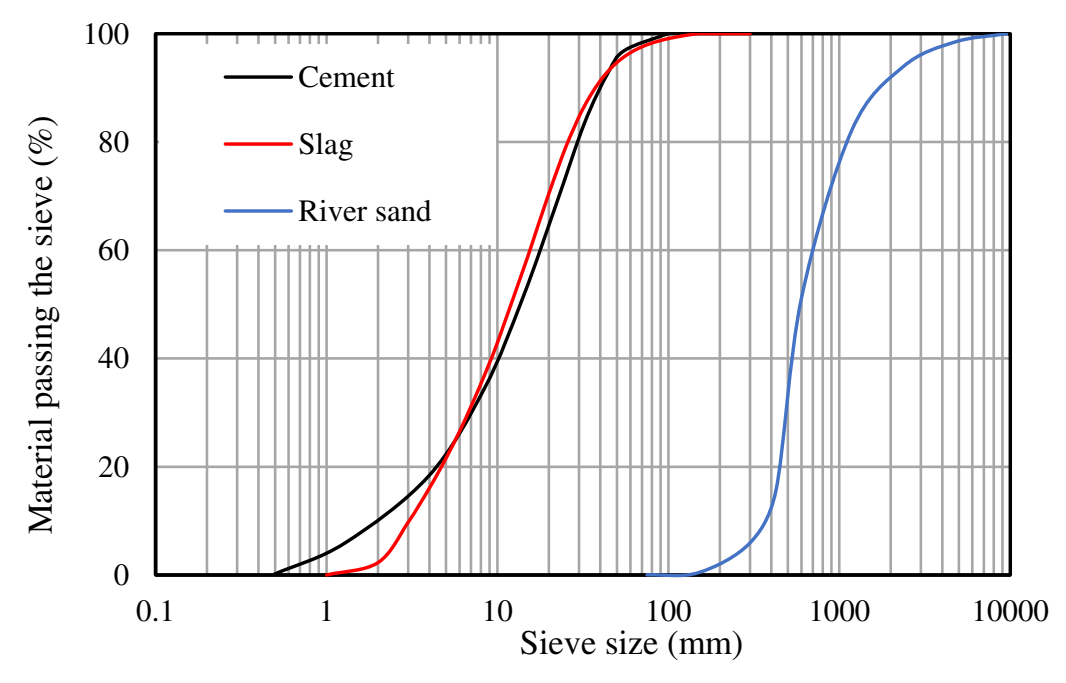


Fig. 1. Particle size distribution of raw materials.

**Table 2** Mixture design of all investigated concretes (kg/m³).

Mixtures	Code	Cement	Slag	RS	HRWR	Water	SF	NC
UHPC	UHPC-Ref	459.0	633.9	965.4	11.0	244.2	156.0	0
	UHPC-0.05 %	459.0	633.9	965.4	11.0	241.9	156.0	2.8
	UHPC-0.10 %	459.0	633.9	965.4	11.0	239.7	156.0	5.6
	UHPC-0.15 %	459.0	633.9	965.4	11.0	237.4	156.0	8.4
	UHPC-0.20 %	459.0	633.9	965.4	11.0	235.2	156.0	11.2
Substrate	SM	739.4	0	1244.1	3.0	295.7	0	0

Note: "RS" refers to river sand; "HRWR" refers to high-range water reducer; "SF" refers to steel fiber; "NC" refers to nanoclay; and "SC" refers to substrate mortar.

slag, and river sand (RS) are shown in Fig. 1. To enhance the crack resistance and toughness, straight steel fibers measuring 0.2 mm in diameter and 13 mm in length were incorporated. The tensile strength and elastic modulus of the steel fiber are 1.9 GPa and 203 GPa, respectively. In order to achieve proper workability, a polycarboxylate-based HRWR was used. The solid content and specific gravity of HRWR are 34.4 % and 1.05, respectively.

# 2.2. Mixture design

The binder of UHPC mixtures consisted of 60 % ground granulated blast-furnace slag (referred as slag in the following sections) and 40 % cement by volume. The w/b was fixed at 0.23 and the dosage of liquid HRWR was 0.62 %, both by mass of binder. The binder-to-sand ratio (b/s) was 1. The addition of nanoclay suspension were 0 %, 0.05 %, 0.10 %, 0.15 %, and 0.20 %, by mass of binders. Steel fibers with a volume fraction of 2 % was used in the UHPC mixtures. In addition, the normal-strength mortar with 0.4 w/c is prepared as the substrate. All the mixture designs are listed in Table 2.

# 2.3. Mixing procedures

The Hobart HL200 mixer was employed to prepare UHPC mixtures according to the following five steps: (1) Step 1: The dry ingredients (cement, slag, and river sand) were introduced to the mixer and mixed at 107 RPM for 2 min; (2) Step 2: The water-based nanoclay suspension was dissolved in 10 % mixing water to form the nanoclay solution, and the HRWR was dissolved in 90 % mixing water to form the HRWR

solution; (3) Step 3: The nanoclay solution and the HRWR solution were gradually added into the mixer within 1 min; (4) Step 4: The mixture was mixed at 107 RPM for 3 min; (5) Step 5: The steel fibers were added to the mixer and mixed at 198 RPM for 2 min. After mixing process, no fiber segregation was found.

The Hobart HL200 mixer was employed to prepare the substrate (i.e., normal-strength mortar) as well. according to the following six steps: (1) a wood mold was first fabricated (length: 228.6 mm, width: 228.6 mm, and height: 76.2 mm); (2) a layer of plastic sheet was covered on the surface of the wood mold before the casting process; (3) the fresh substrate (i.e., normal-strength mortar) was cast into the mold to 50.8-mm thickness; (4) the 2-min vibration was applied to ensure the smoothness of the substrate surface; (5) the substrate was demolded after one day and equally cut into 9 small specimens (length: 76.2 mm, width: 76.2 mm, and height: 50.8 mm); (6) the prepared substrate specimens were cured into the water tank until 28 days.

## 3. Experimental method

The experimental methods are introduced in Sections 3.1 to 3.5 to evaluate the effect of water-based nanoclay suspension on the key performances of UHPC. The methods to investigate the synergy effects of water-based nanoclay suspension and vibration on the interfacial properties between UHPC overlay and substrate are presented in Sections 3.6 and 3.7, respectively.

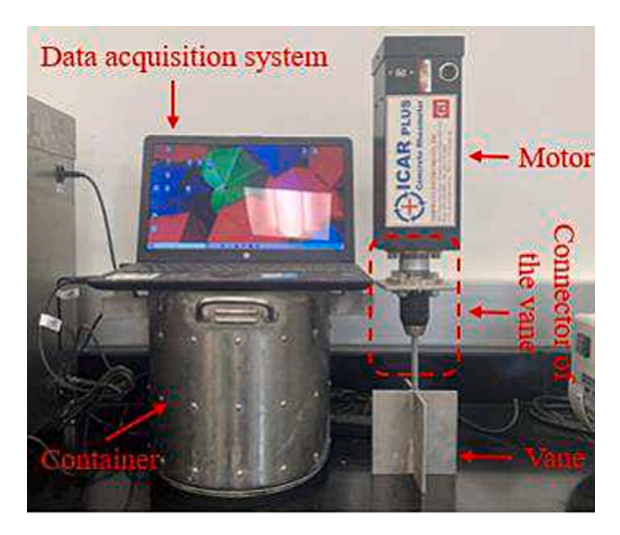


Fig. 2. The ICAR rheometer for the measurement of mixing torque and rheological properties.

# 3.1. Mixing torque evaluation, rheology measurements, and thixotropy evaluation

An ICAR rheometer (Fig. 2) was applied to measure the mixing

torque during the mixing process as well as the dynamic yield stress and static yield stress of the homogenized UHPC mixtures. All measurements were performed three times to make sure of the reproducibility of the results. For the ICAR rheometer, the diameter and height of the container are both 280 mm, and both the diameter and height of the vane are 127 mm.

# 3.1.1. Quantitative evaluation of mixing torque

In order to understand the effect of adding water-based nanoclay on the mixing difficulty of UHPC production, the evolution of mixing torques of UHPC during the mixing process was evaluated. The mixing torques of the UHPC mixtures were measured by the ICAR rheometer. Specifically, the Hobart mixer was used to mix the UHPC in this research and the 2-minutes dry mixing process was excluded from the mixing torque measurement. The integral procedures are divided as four steps shown in Fig. 3: (1) When all mixing water and HRWR were added into the mixer, the Hobart mixer was stopped every 30 s and the mixing bowl was taken out; (2) The ICAR motor connected with the mixing vane was put into the mixing bowl to start the measurement (note: the peak value of the development of the mixing torque at each moment was recorded); (3) The ICAR motor connected to the mixing vane was removed and the mixing bowl was put back to the mixer to restart the mixing process. (4) The step (1–3) was repeated until the mixing torque was stabilized.

As shown in Fig. 4, the representative curve shows that the mixing torque evolution can be divided into two stages, including mortar homogenization and UHPC homogenization. The dramatic increment of the mixing torque was mainly happened in Stage I (i.e., mortar homogenization process). Afterwards, the addition of steel fibers in Stage II

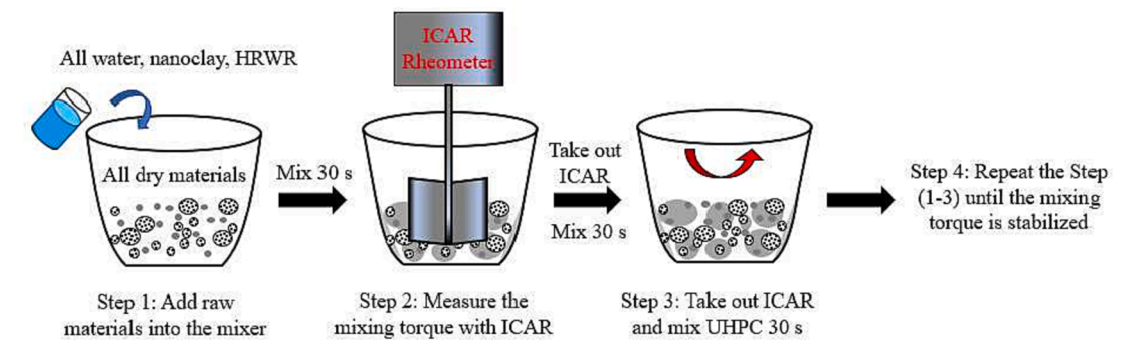


Fig. 3. The illustrative figure of the mixing torque measurement.

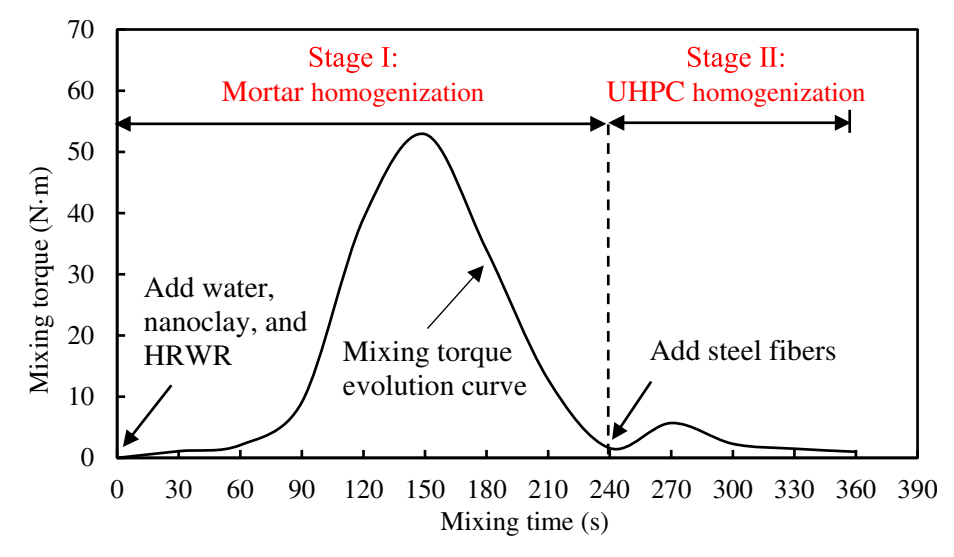


Fig. 4. The representative evolution of mixing torque during the UHPC mixing process.

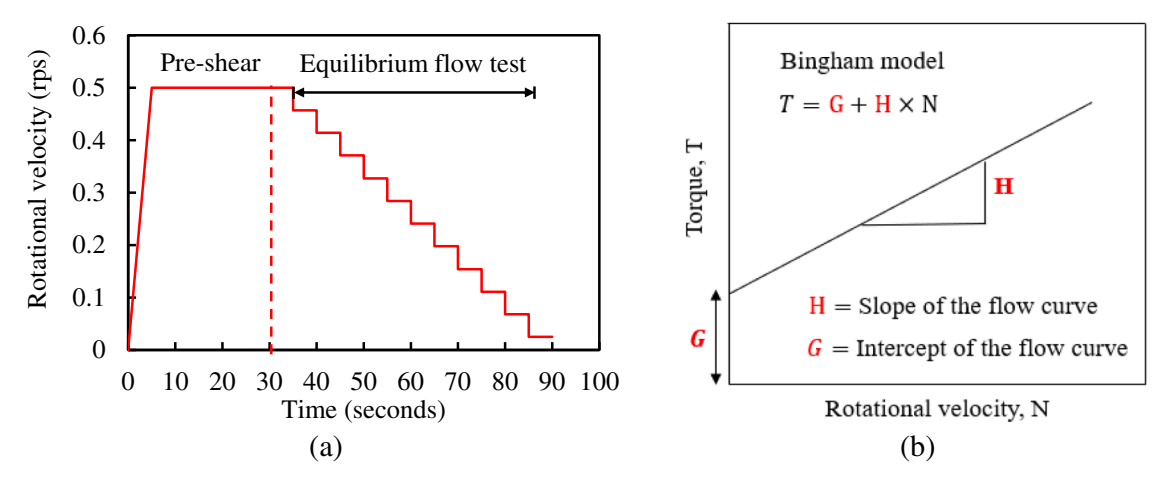


Fig. 5. The test for dynamic yield stress: (a) equilibrium flow curve; (b) the Bingham model.

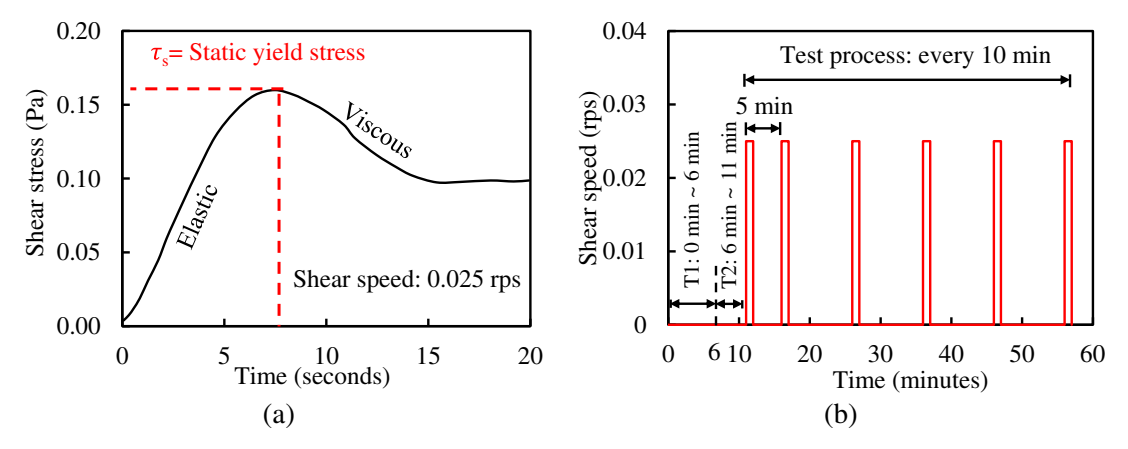


Fig. 6. The test for static yield stress: (a) shear-rate-control method; and (b) the time instant of static yield stress measurement. "T1" and "T2" refer to the time for mixing and rest, respectively.

(i.e., UHPC homogenization process) had negligible contribution on the evolution of the mixing torque.

# 3.1.2. Protocols to determine dynamic yield stress

The dynamic yield stress is defined as the minimum stress required for maintaining flow. In this study, the time zero of the dynamic yield stress evaluation (see Fig. 4) refers to the time when the liquid materials (i.e., water, nanoclay, and HRWR) are added into the mixer, and it should be pointed out that the 2-minute dry mixing process is excluded in the time. The first dynamic yield stress test is conducted after the homogenization of UHPC mixtures (i.e., 6 min after the water is added into the mixer). According to preliminary study, all UHPC mixtures in this study could be homogenized after 6 min. To determine the coupled effects of time and nanoclay content, the dynamic yield stresses for all investigated UHPC mixtures were measured at 6 min, 16 min, and 56 min, respectively. Detailed procedures were introduced as follows: (1) Step 1: the UHPC mixtures were pre-sheared at 0.5 rps for 25 s. (2) Step 2: the rotation speed gradually decreased from 0.5 rps to 0.025 rps in 12 steps. For each step, the rotation speed was kept for 5 s (Fig. 5(a)). (3) Step 3: the steady state of torque values was fitted by the Bingham model (see Fig. 5(b)). (4) Step 4: the Reiner-Riwlin transformation equation was used to calculate the dynamic yield stress [66], as shown in Eq. (1) and Eq. (2).

$$T = G + H \times N \tag{1}$$

$$\tau_d = \frac{\left(\frac{1}{R_i^2} - \frac{1}{R_o^2}\right)}{4 \times \pi \times h \times \ln\left(\frac{R_o}{R_i}\right)} \times G \tag{2}$$

where T is the torque (N·m); G is the intercept of the flow curve (N·m); H is the slope of the flow curve (N·m/s); N is the rotational velocity (rps);  $\tau_d$  is the dynamic yield stress (Pa);  $R_i$  is the inner cylinder radius of the coaxial cylinders (m);  $R_o$  is the outer radius of the container (m); and h is the height of the inner cylinder submerged in the materials in the rheometer (m).

# 3.1.3. Protocols to determine static yield stress

The static yield stress is defined as the stress required for initiating flow. The time zero of the static yield stress evaluation (see Fig. 4) refers to the time when the liquid materials (i.e., water, nanoclay, and HRWR) are added into the mixer. As shown in Fig. 6(a), a shear-rate-control method [67] was used to determine the static yield stress of UHPC mixtures. The shear rate was fixed at 0.025 rps; the static yield stress was determined as the vertical value of the peak value of the measured curve. To quantify the thixotropy, the static yield stresses of all investigated UHPC mixtures were measured at 11 min, 16 min, 26 min, 36 min, 46 min, and 56 min, respectively. As shown in Fig. 6(b), detailed procedures were introduced as follows: (1) Step 1: the homogenized UHPC mixtures were poured into the container and rested to eliminate the shear history; (2) Step 2: the first test started at 11 min after water addition (i.e., 5 min rest after the homogenization), and a shear speed of 0.025 rps was kept for 30 s; (3) Step 3: the second test started at 16 min

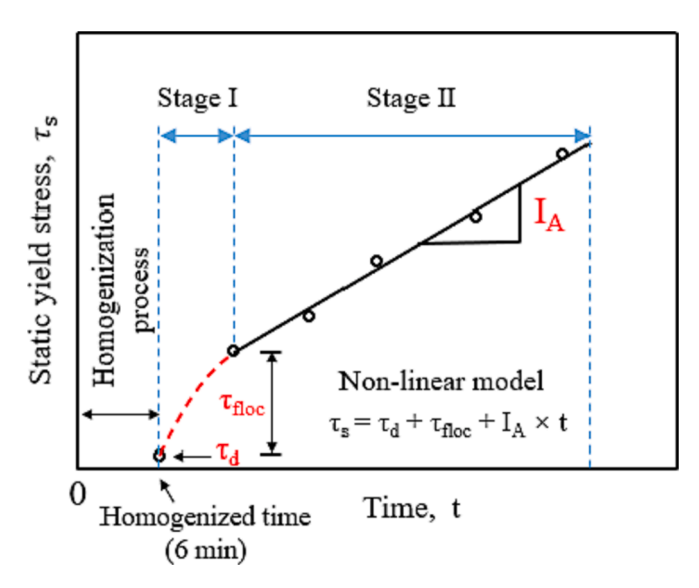
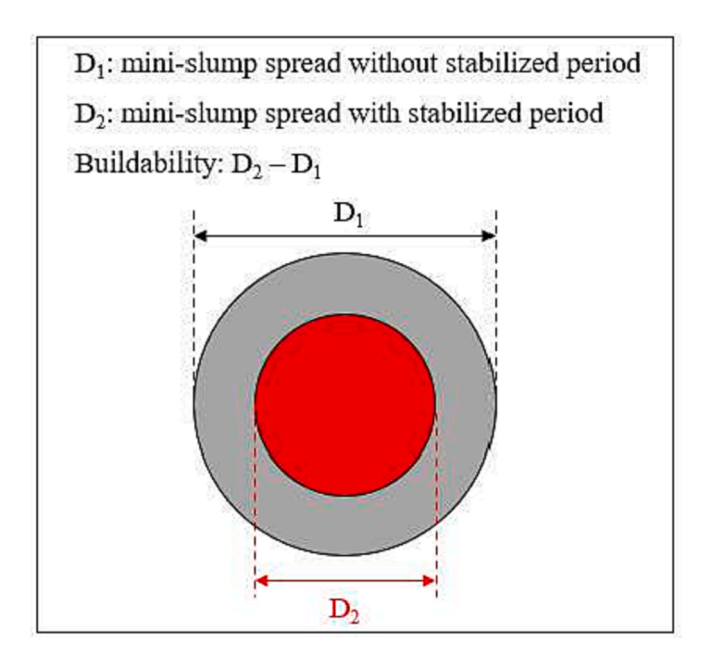


Fig. 7. Determination of thixotropic properties for UHPC mixtures.



 ${f Fig.~8.}$  The definition of buildability: the difference from the mini slump spread values.

(i.e., 10 min rest after the homogenization), at which the significant initial fluctuation of the static yield stress occurred; (4) Step 4: the tests were repeated every 10 min until the 56 min. The equation used to calculate the static yield stress from the torque was shown in Eq. (3) and Eq. (4) [68].

$$\tau_s = T_{max}/K \tag{3}$$

$$K = 2 \times \pi \times r^2 \times (h + \frac{1}{3} \times r) \tag{4}$$

where  $\tau_s$  is the static yield stress,  $T_{max}$  is the max torque value, and h and r are the filling height and radius of the vane (m), respectively.

# 3.1.4. Evaluation of thixotropy

The thixotropy of UHPC mixtures was quantified by evaluating the yield stresses determined from Section 3.1.2 and Section 3.1.3. As shown in Fig. 7, the yield stress first increased rapidly in Stage 1 after the

homogenization, then the increased rate dropped and the relations between the static yield stress and time followed a linear line in Stage 2. This trend is similar with results proved by Mostafa and Yahia [69], Roussel [70], and Teng et al. [44]. The evolution of the yield stress with time can be fitted by a non-linear model proposed by Ma et al. [45], as shown in Eq. (5). However, it should be acknowledged that the development trend is highly dependent on the specific UHPC mixture designs. Ma and Kawashima [48] found out that the static yield stress of their mixture design increases exponentially with time after the first hour. Hence, this study focuses on the evolution of the static yield stress within one hour.

$$\tau_s = \tau_d + \tau_{floc} + I_A \times t \tag{5}$$

where t is the testing time starting from the end of mixing;  $\tau_s$  is the static yield stress at t;  $I_A$  is the thixotropy index;  $\tau_d$  is the dynamic yield stress; and  $\tau_{floc}$  is the initial fluctuation between dynamic yield stress and the first measurable static yield stress due to the particle flocculation.

#### 3.2. Workability and buildability test

The workability and buildability of UHPC mixtures were evaluated by the mini-slump spread test according to ASTM C1437 [71]. Specifically, these tests were conducted without any jolting. For the workability test, the mini-slump cone was lifted immediately after filling up with the UHPC. Then the diameters were measured until the flow stayed stable. For each UHPC mixture, the workability test was conducted at 6 min, 16 min, and 56 min after all mixing water is added into the mixer. To obtain the irreversible workability loss of thixotropic UHPC mixtures, the investigated mixtures were kept mixing at 59 RPM to eliminate the flocculation until each test.

In addition, buildability is essential during the construction process, which is closely related to the shape stability of fresh UHPC after the placement [37,72]. In this study, the mini-slump cone was filled and then lifted after 10 min for the buildability test. The buildability is defined as the difference of mini slump spread values measured with and without shape stabilized period (10 min), as shown in Fig. 8. The buildability test was conducted for evaluating the structural build-up properties of the thixotropic UHPC mixtures [73].

# 3.3. Compressive strength test

The compressive strengths of UHPC mixtures at 1, 3, 7, 14, and 28 days were evaluated using 50-mm cubes, according to ASTM C109 [74]. Three sample replicates were prepared for each test, and the average results for each test were reported.

# 3.4. Autogenous shrinkage test

The autogenous shrinkage of UHPC mixtures was evaluated in accordance with ASTM C1698 [75]. The final setting time was set as time zero. The test was on a daily basis for the first week and on a weekly basis until 28 days. The prism specimens measuring 25 mm  $\times$  25 mm  $\times$  280 mm were sealed with water-proof alumina tap to prevent moisture loss. Three sample replicates were prepared for each test, and the average results for each test were reported.

# 3.5. Hydration heat test

The hydration heat evolution was evaluated by using an isothermal calorimeter (model: Calmetrix I-Cal 4000 HPC), which was programmed to maintain the samples at 25 °C. About 60 g of fresh UHPC was sealed in a plastic vial and placed into the calorimeter. The heat of hydration data was measured 2 min after the end of mixing and continuously measured for 36 h. The results were normalized by the mass of the binder.

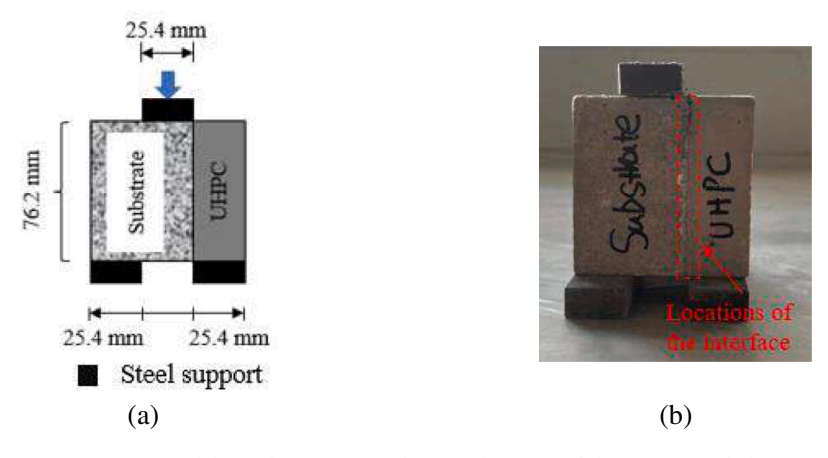


Fig. 9. Test setup of direct shear test: (a) schematic diagram and (b) experimental photo.

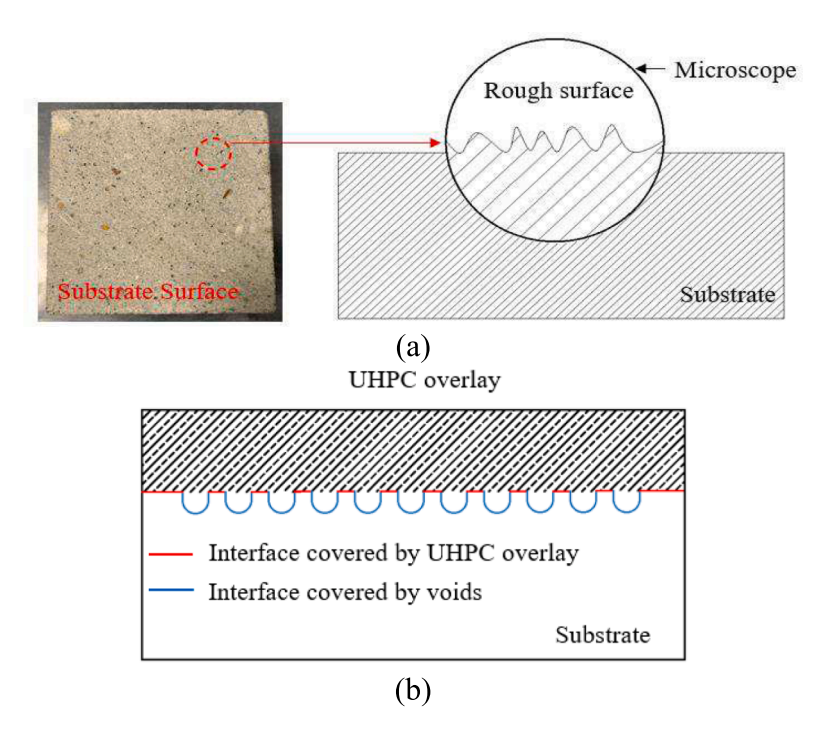


Fig. 10. Schematic diagram of (a) the substrate surface and (b) the interface between UHPC overlay and substrate concrete.

## 3.6. Interfacial properties test

In this study, the direct shear test [76] was employed to evaluate interfacial properties between UHPC overlay and substrate, and the test set-up is shown in Fig. 9. Previous researchers revealed that the proper vibration could improve the interface quality between UHPC overlay and substrate, but the effect was not quantified and well understood [19]. Therefore, the effect of vibration on the interfacial properties was investigated in this study. Two vibration parameters were considered: (1) vibration amplitude (i.e., 0.79 mm and 1.58 mm); (2) vibration time (i.e., from 0 s to 60 s).

For the direct shear test, the bond strength was reported, which is represented by dividing the maximum load F by the area of failure surface, as shown in **Eq.** (6):

$$F_b = \frac{F}{2bd} \tag{6}$$

where  $F_b$  is the bond strength; F is the maximum load; b and d are the width and height of the cube, respectively.

## 3.7. Microstructural analysis

The microstructural analysis of the interface between UHPC overlay and substrate (shown in Fig. 9(b)) was examined using small samples with an approximate dimension of 20 mm  $\times$  20 mm  $\times$  20 mm, which were cut from shear test samples. After 28 days of curing, the samples were soaked in isopropanol to stop further hydration, then vacuum dried for 24 h. Then, samples were vacuum impregnated with low-viscosity epoxy resin. In addition, silicon carbide papers and polishing cloth were applied to grind and polish the samples. Finally, the prepared samples were coated with carbon and examined using the microscope (model: Zeiss Auriga FIB/SEM with a back-scattered detector).

The microscope was operated at 5 kV at 10 mm distance. A 40x magnification was used to obtain the view of interface microstructure on different areas. All images were stitched together to form the entire map of interface. Due to a certain degree of roughness on the surface of substrate, as shown in Fig. 10(a), the thixotropic UHPC may not be able to fully contact with the substrate, which formed voids on interface, shown in Fig. 10(b). These voids can further weaken the interfacial

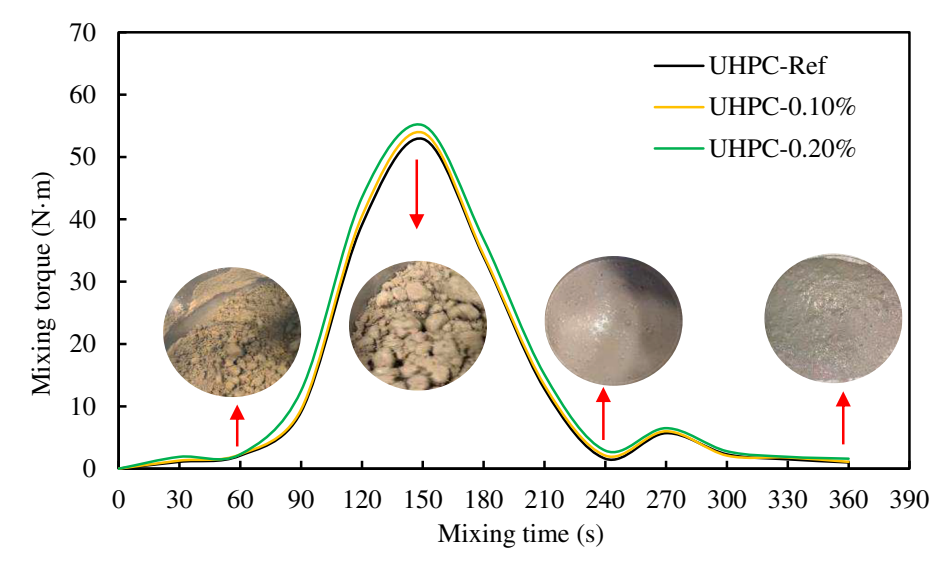


Fig. 11. Mixing torque-time curves of UHPC with different water-based nanoclay contents.

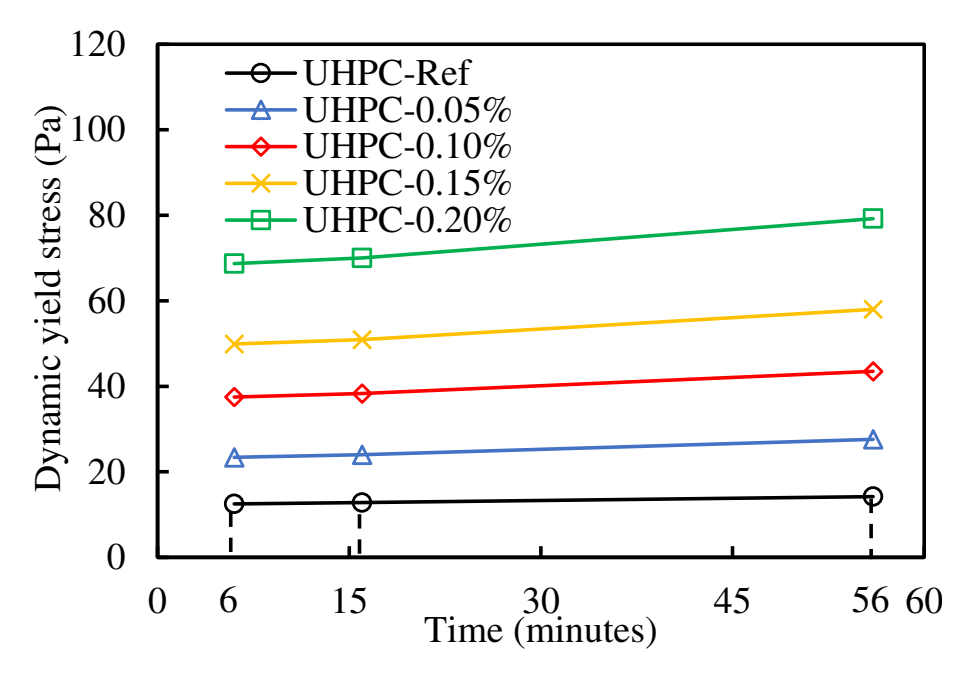


Fig. 12. Dynamic yield stress of UHPC with different water-based nanoclay contents over time.

quality.

The index  $P_{voids}$  was proposed to evaluate the interface quality.  $P_{voids}$  is defined as the ratio of the interface length covered by air voids to the total length of the interface, as shown in Eq. (7). For each mixture, at least 10 independent samples were scanned and calculated, and the average value was reported.

$$P_{voids} = \frac{L_{blue}}{L_{blue} + L_{red}} \tag{7}$$

where  $P_{voids}$  is the percentage of the interface length covered by air voids, as shown in Fig. 8(b);  $L_{blue}$  is defined as the interface length covered by air voids; and  $L_{blue} + L_{red}$  is the total interface length of investigated samples.

## 4. Results and discussion

Section 4.1 introduces the effect of water-based nanoclay suspension

on the performance of UHPC and discusses the underlying mechanism. Section 4.2 elaborates the synergy effects of water-based nanoclay suspension and vibration on the interfacial properties between UHPC overlay and substrate and investigates the underlying mechanism.

# 4.1. Effect of nanoclay content on performance of UHPC

# 4.1.1. Effect of nanoclay content on mixing kinetics of UHPC

Adding nanoclay might increase the mixing torque during the UHPC mixing process, which increases the mixing difficulty and affects the mixing efficiency for the large-scale UHPC production on job sites. Therefore, in this section, the effects of nanoclay content on mixing kinetics of UHPC were investigated.

Fig. 11 plots the mixing torque versus mixing time curves for the investigated UHPC mixtures, which reflect the evolution of the mixing torque throughout the mixing process. From 0 s to 60 s, mixing torque was slightly increased after the HRWR solution and nanoclay solution were added into the mixer. From 60 s to 240 s, the mixing torque was

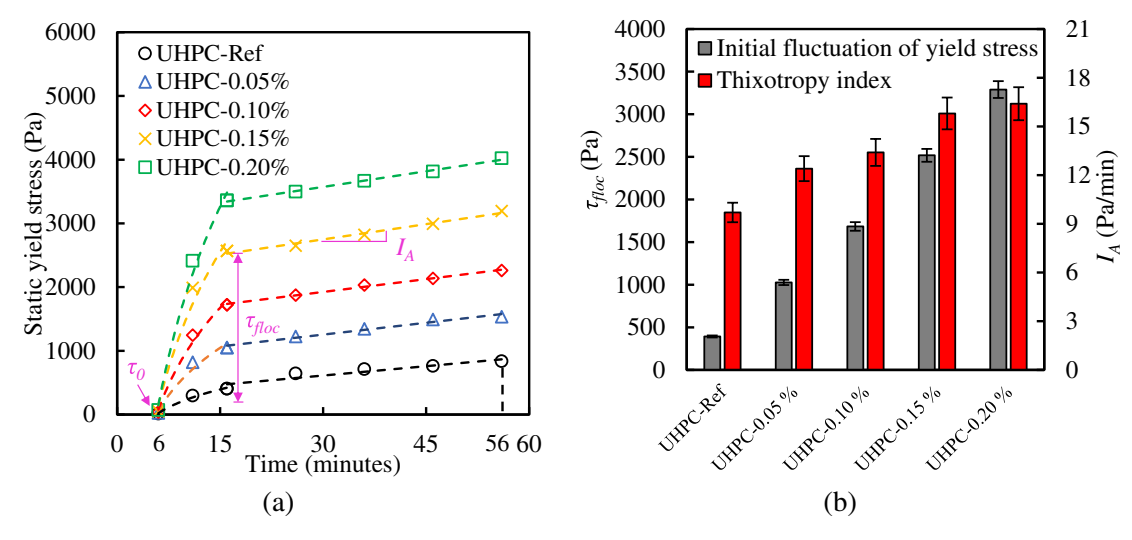


**Fig. 13.** The results of initial increase of static yield stress ( $\tau_{floc}$ ) and thixotropy index ( $I_A$ ): (a) the non-linear relationship; and (b) the summaries of calculated results.

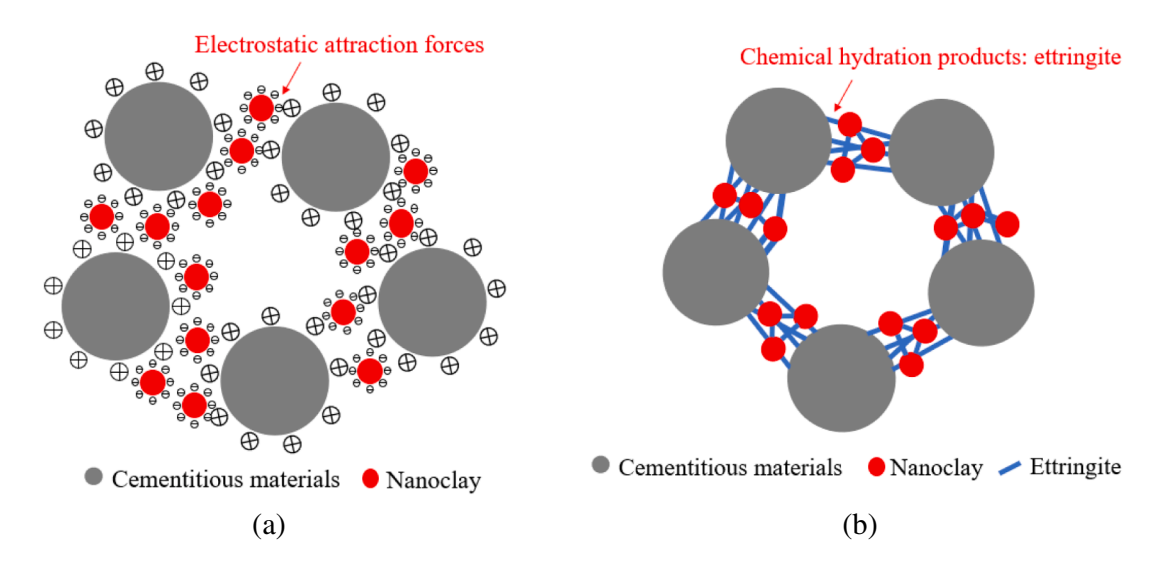
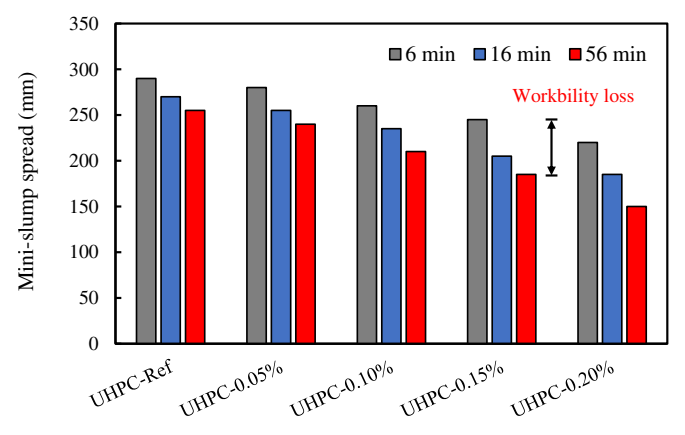


Fig. 14. The mechanisms of water-based nanoclay on the thixotropy development: (a) physical effect: accelerated flocculation (reversible); (b) chemical effect: hydration reaction (irreversible).



**Fig. 15.** Results of workability loss of UHPC with different water-based nanoclay contents.

significantly increased, then decreased, and finally stabilized, which attributes to the evolution of microstructure for powder-liquid mixtures [77,78]. The UHPC mixture transformed from powders to homogenized mortar was defined as the mortar homogenization progress. The results indicated that, as the water-based nanoclay content increased from 0 to 0.20 %, the maximum mixing torque only increased by 3 % (from 53.9 N·m to 55.1 N·m) and the homogenization time remains the same. From 240 s to 360 s, the mixing torque was slightly increased, then decreased, and finally stabilized, which was attributed to the addition of steel fibers. Therefore, the homogenization time for all UHPC mixtures is approximately 6 min. From the determined maximum mixing torque and homogenized time of the investigated mixtures, it can be concluded that adding water-based nanoclay suspension has negligible effects on the mixing difficulty and efficiency of the UHPC production.

#### 4.1.2. Effect of nanoclay content on thixotropic properties of UHPC

The thixotropy of cement-based materials within one hour is an important property that represents the ease of casting and the stability of concrete after casting. Besides, the thixotropy of cement-based materials is caused by reversible effects (i.e., physical particles flocculation) and irreversible effects (i.e., chemical hydration reaction) [67]. Billberg [79]

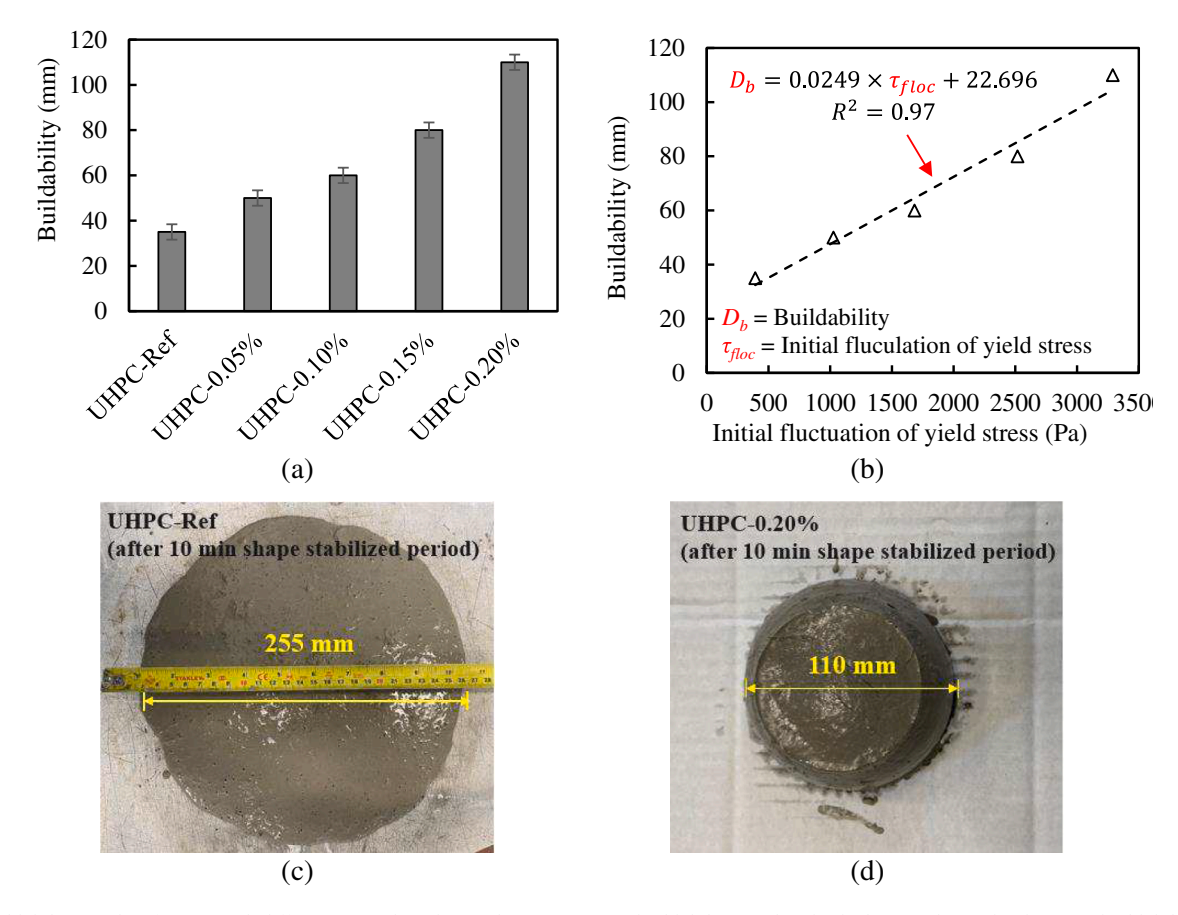
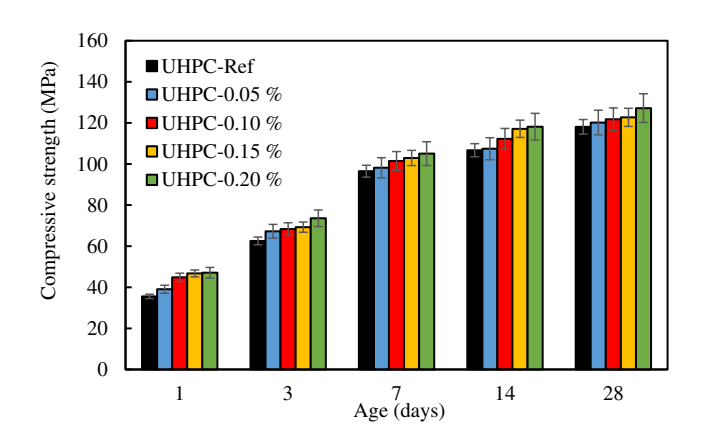


Fig. 16. Buildability results of UHPC with different water-based nanoclay contents: (a) buildability results; (b) the linear relationship between buildability and initial fluctuations of static yield stress; (c) spread flow of UHPC-Ref after 10 min shape stabilized period; and (d) spread flow of UHPC-0.20 % after 10 min shape stabilized period.



 $\begin{tabular}{ll} Fig. \ 17. \ Compressive \ strength \ results \ of \ UHPC \ with \ different \ water-based \ nanoclay \ contents. \end{tabular}$ 

ascribed the irreversible effects to the development of the dynamic yield stress, and the sum of irreversible effect and reversible effect to the development of the static yield stress. Therefore, in this section, the development of yield stress was investigated to elaborate the effect of nanoclay suspension content on the thixotropic properties of UHPC.

Fig. A1 in Appendix shows the flow curves measured with stepwise rotation speed at 6 min, 16 min, and 56 min after the end of homogenization, respectively. The data points are fitted using the Bingham model [80]. Fig. 12 summarizes the dynamic yield stress for UHPC with different nanoclay contents at different time instants. The figure indicates that, at 6 min, the dynamic yield stress of UHPC mixtures

increases from 12.5 Pa to 68.6 Pa as the water-based nanoclay content increases from 0 to 0.20 %. The results indicate that adding nanoclay accelerates the hydration process, which was further validated in Section 4.1.4 [81]. Variations in dynamic yield stress curves are also in good agreement with the results from Teng et al. [44].

The development of the dynamic yield stress is also related to the test time. As the test time increased from 6 min to 16 min, the dynamic yield stresses of UHPC mixtures were increased from 12.5 Pa to 12.8 Pa (by 2 %), 37.5 Pa to 38.3 Pa (by 2 %), and 68.7 Pa to 70.0 Pa (by 2 %) for UHPC-Ref, UHPC-0.10 %, and UHPC-0.20 %, respectively. Hence the increments of the dynamic yield stresses from 6 min to 16 min were negligible. Then, as the test time increased from 16 min to 56 min, the dynamic yield stresses of UHPC mixtures were increased from 12.8 Pa to 14.2 Pa (by 11 %), 38.3 Pa to 43.5 Pa (by 14 %), and 68.7 Pa to 79.2 Pa (by 15 %) for UHPC-Ref, UHPC-0.10 %, and UHPC-0.20 %, respectively. The increments of the dynamic yield stresses from 16 min to 56 min were much more significant. The results indicated that the irreversible effect was negligible within 10 min after the homogenization (i.e., from 6 min to 16 min), but gradually became significant when test time was over 10 min. This phenomenon can be attributed to the effect that more hydration products were generated, and dynamic yield stresses were increased with the increase of test time [82].

To measure the static yield stresses of UHPC mixtures, the shear stresses versus corresponding shear time were investigated based on the shear-rate-control method. The ranges for water-based nanoclay content and test time are from 0 to 0.20 % and from 11 min to 56 min, respectively. The derived shear stress-shear time evolution curves were plotted in Fig. A2 in Appendix. It should be noted that the peak values of shear stress in these curves represent the static yield stress. Because the static yield stress after the homogenization (i.e., 6 min) is too low to be

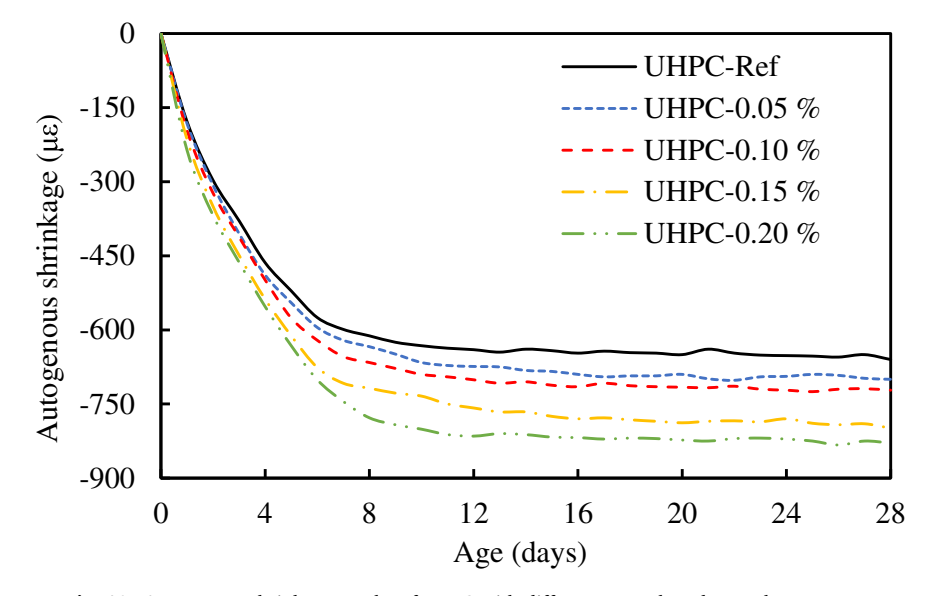


Fig. 18. Autogenous shrinkage results of UHPC with different water-based nanoclay contents.

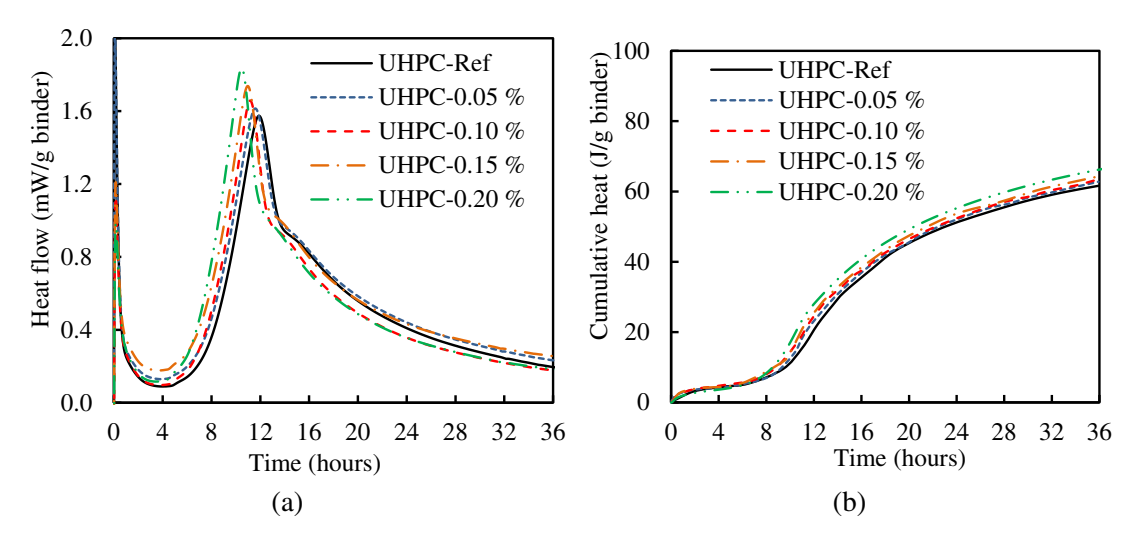


Fig. 19. Hydration heat results of UHPC with different nanoclay contents: (a) heat flow evolution; and (b) cumulative heat.

measured, the initial dynamic yield stress is considered as the static yield stress [44]. As defined in Section 3.1.4, the thixotropy of the investigated UHPC mixtures were evaluated by the evolutions of the static yield stresses. Fig. 13(a) shows the non-linear relationship between static yield stress and test time. The difference between the initial dynamic yield stress and static yield stress at 16 min reflects the initial fluctuation of the yield stress ( $\tau_{floc}$ ). The slope of the static yield stress from 16 min to 56 min reflects the thixotropy index ( $I_A$ ). Fig. 13(b) summarizes the calculated results of  $\tau_{floc}$  and  $I_A$ .

Fig. 13 indicated that, as the water-based nanoclay content increased from 0 to 0.20 %, the initial fluctuation of yield stress ( $\tau_{floc}$ ) and the thixotropy index ( $I_A$ ) were increased from 392.7 Pa to 3290.0 Pa and from 9.7 Pa/min to 16.4 Pa/min, respectively. The results reveal that the yield stress of UHPC mixtures was significantly increased by increasing water-based nanoclay content in the first 10 min after mixing. After reduction in the increasing rate, the static yield stress increased linearly with time. The evolution trend is in a good agreement with the result conducted by Kawashima et al. [47]. The underlying mechanisms are elaborated in the following:

In Stage I (6  $\sim$  16 min), the initial fluctuations of static yield stresses were significantly increased with the nanoclay addition. As introduced

before, the structural build-up of fresh UHPC is related to the sum of reversible effect (i.e., physical particles flocculation) and irreversible effect (i.e., chemical hydration reaction). Results (shown in Fig. 12) showed that the negligible development of the dynamic yield stress in Stage I, which indicated the irreversible effect in Stage I was limited [79]. Therefore, the structural build-up of fresh UHPC in Stage I was ascribed to reversible effect (i.e., particles physical flocculation). Specifically, cement particles are electrostatically attracted by negative charged surface of the nanoclay particles shown in Fig. 14(a), accelerating the flocculation [51]. In this case, the significant development of the initial static yield stress in the first few minutes improved the shape stability of fresh UHPC after the placement.

In Stage II (16  $\sim$  56 min), the growth rate of static yield stress was significantly slowing down (shown in Fig. 13). It was speculated that the further improvement of the structural build-up of fresh UHPC came from the irreversible effect (i.e., chemical hydration reaction). Results (shown in Fig. 12) also validated the irreversible effect in Stage II because the dynamic yield stress in Stage II increased around 15 %. The underlying mechanism is the nanoclay has high content of aluminates, which alters the sulfate-aluminate balance in the solution, leading to high amount of ettringite due to the secondary hydration of  $C_3A$  (shown in Fig. 14(b))

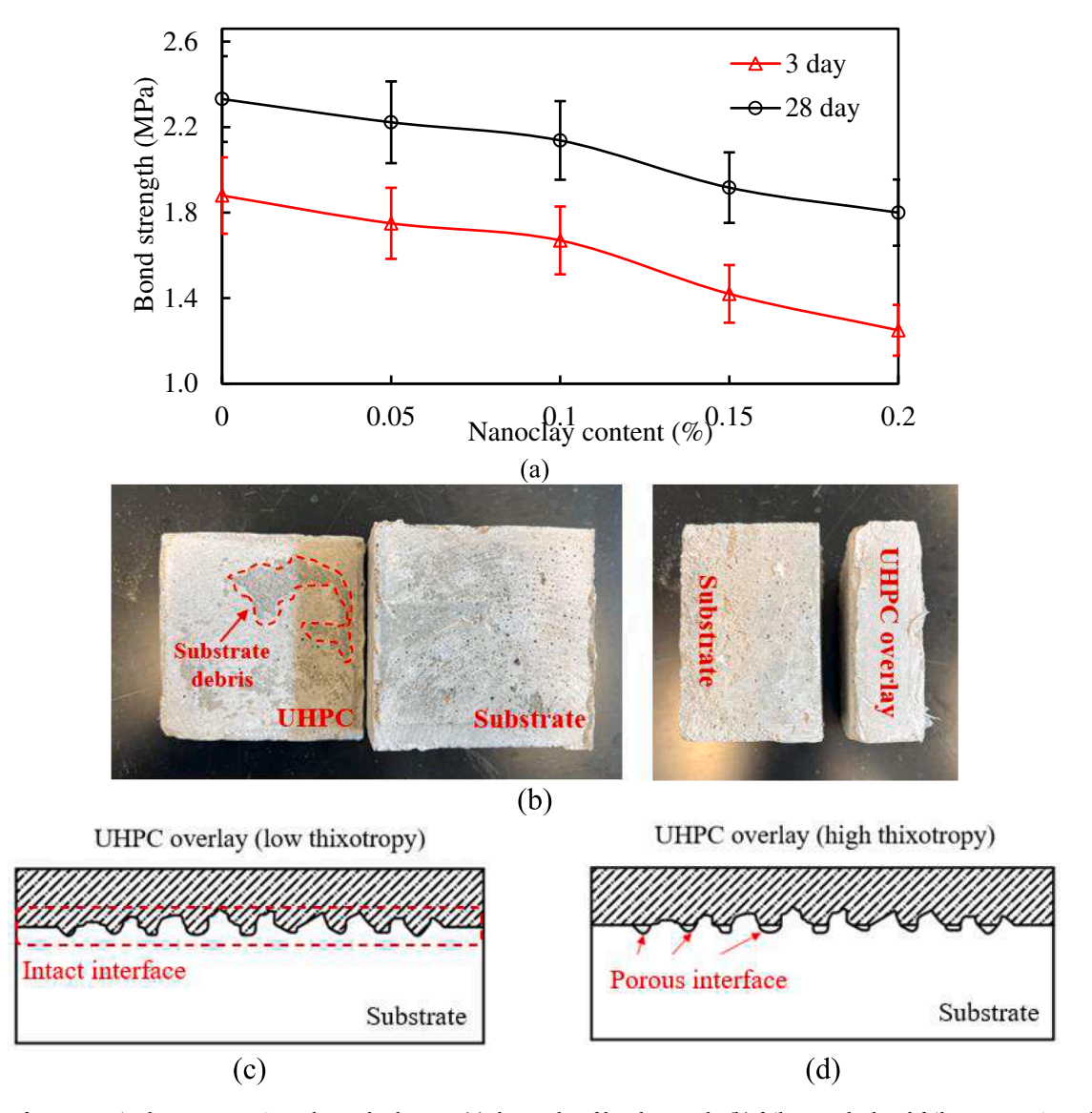


Fig. 20. The interface properties between UHPC overlay and substrate: (a) the results of bond strength; (b) failure mode: bond failure at UHPC overlay/substrate interface; and (c-d) the speculated interface. Note: the data points in this figure are the average value of three parallel experiments.

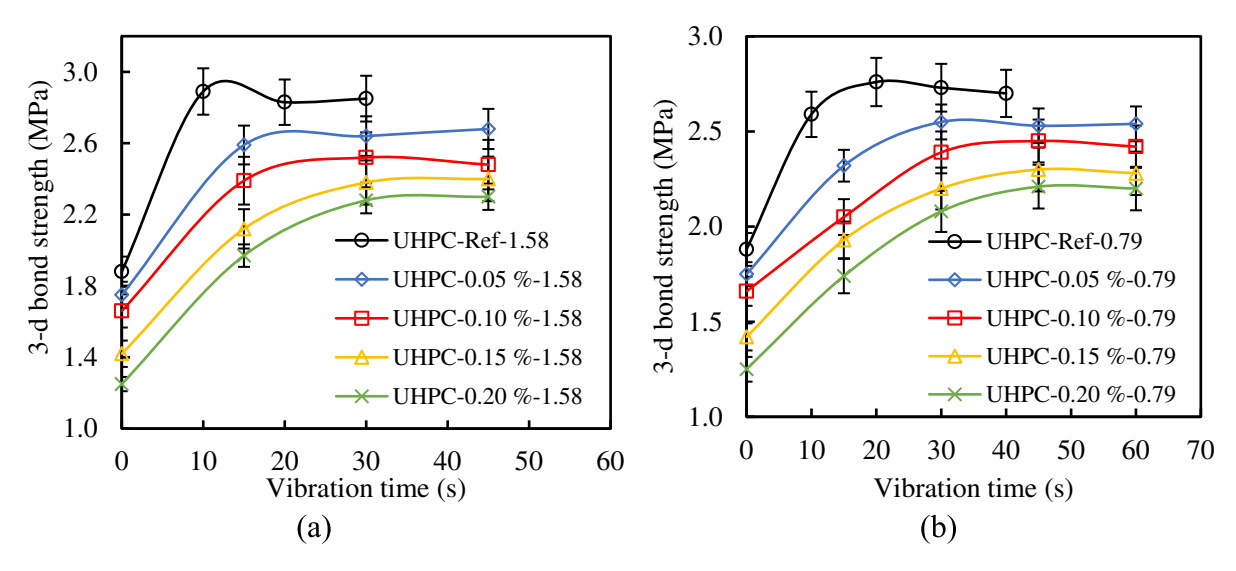
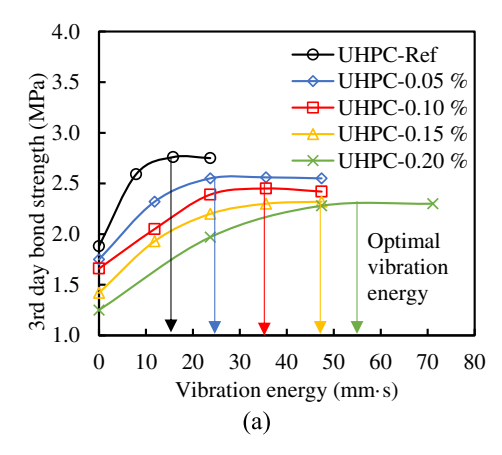


Fig. 21. The effect of vibration on bond strength of UHPC overlay with different water-based nanoclay contents: (a) 1.58 mm amplitude; and (b) 0.79 mm amplitude. Note: the data points in this figure are the average value of three parallel experiments.



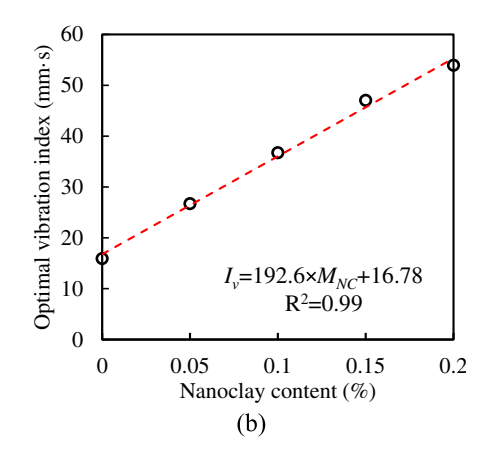


Fig. 22. The established relationship between: (a) vibration index and bond strength; and (b) water-based nanoclay contents and optimal vibration index.  $M_{NC}$  represents the nanoclay content by mass of binder. Note: the data points are the average value of three parallel experiments.

[83]. In summary, the development of the structural build-up in Stage II was ascribed to the sum of reversible effect (i.e., physical particles flocculation) and irreversible effects (i.e., chemical hydration reaction). It should be noted that the seeding effect of nanoclay for chemical hydration reaction is not considered for the investigated period, because the precipitation and growth of CH and C—S—H usually occurred after the dormancy phase of cement hydration (around 4 h after water addition) [84]. The reduced increase rate of static yield stress in Stage II benefits to have longer efficient construction time because the lower shear stress is required for initiating flow of UHPC.

#### 4.1.3. Effect of nanoclay content on workability and buildability

The workability of cement-based materials is closely related to the construction quality. Poor workability might result in poor compaction and difficult placement [85,86]. Fig. 15 plots the workability results of investigated UHPC mixtures over time. The mini-slump spread of UHPC mixtures was decreased with the increases of water-based nanoclay content. For instance, as the water-based nanoclay content increased from 0 to 0.20 %, the mini-slump spread of investigated UHPC mixtures was reduced from 290 mm to 220 mm (by 24 %) when the test time was at 6 min (i.e., right after the mixing process) because the nanoscale nanoclay particles fill in the gaps among cement, slag, and river sand particles to increase the internal frictions between particles [51]. The use of nanoclay also expedites the loss of workability. As the nanocaly content increased from 0 to 0.20 %, the mini-slump loss (i.e., the difference between the mini-slump spread at 6 min and at 56 min) was further increased from 35 mm to 70 mm. The mini-slump loss over time was due to the formation of hydration products (e.g., ettringite), which consumes the free water and has strong affinity to absorb HRWR [87].

The buildability of cement-based materials is closely related to the shape stability after the placement. Better buildability helps the fresh UHPC maintain its shape instead of freely flowing on the bridge deck overlay [37]. The definition of the buildability is defined in Section 3.2. As shown in Fig. 16(a), the buildability was improved with the increase of water-based nanoclay content. For instance, as the water-based nanoclay content increased from 0 to 0.20 %, the buildability was increased from 35 mm to 110 mm (by 215 %), which can be attributed to the improved thixotropy, especially the high initial fluctuations of static yield stress due to the use of nanoclay. The increased static yield stress can efficiently resist the gravity to keep the shape stably [88]. A linear relationship between the buildability and initial fluctuations of static yield stress was observed in Fig. 16(b). A mixture with higher initial fluctuation of static yield stress results in higher buildability and better shape stability. Fig. 16(c) and Fig. 16(d) show the spread flow of investigated UHPC mixtures (i.e., UHPC-Ref and UHPC-0.20 %) after the shape stabilized period.

The use of water-based nanoclay benefits applying UHPC as an

overlay. During the mixing, adding water-based nanoclay suspension has limited effect on the development of mixing torque and the homogenization time compared with UHPC without nanoclay, which indicates adding water-based nanoclay has negligible effect on the mixing difficulty and mixing efficiency for UHPC production. When the mixing was completed, the dynamic yield stress of UHPC mixtures was still low, which further facilitates the casting/placing process. Afterwards, the static yield stress builds up quickly, which helps keep the shape of UHPC mixtures on sloped structures.

#### 4.1.4. Effect of nanoclay content on hardened properties of UHPC

Fig. 17 plots the compressive strengths of investigated UHPC mixtures from 1 day to 28 days. As the water-based nanoclay contents increased from 0 to 0.20 % by mass of binder, the compressive strength at 1 day was increased from 39.0 MPa to 47.1 MPa (by 21 %), the compressive strength at 7 days was increased from 96.5 MPa to 105.1 MPa (by 9 %), and the compressive strength at 28 days was increased from 118.1 MPa to 127.2 MPa (by 7 %). The results indicates that the addition of water-based nanoclay enhances compressive strength, especially at early ages. It was speculated that the presence of nanoclay particles in UHPC mixtures can serve as seeds to provide new nucleation sites to promote hydraulic reaction [44,89]. This underlying mechanism is also proved by Huang et al. [90] and Teng et al [44] who revealed that the UHPC matrix was densified due to the higher hydration degree, resulting in an improvement in compressive strength. Besides, the speculation was also validated by the measurement of hydration heat test in this study.

Fig. 18 plots the results of autogenous shrinkage of the investigated UHPC mixtures from 1 day to 28 days. As the water-based nanoclay contents increased from 0 to 0.20 %, by mass of binder, the autogenous shrinkage at 28 days was increased from 660  $\mu\epsilon$  to 829  $\mu\epsilon$  (by 25 %). The results showed that the addition of water-based nanoclay significantly increased the autogenous shrinkage. There exists two main underlying mechanisms: (1) the refinement of pore size by adding nanomaterials can exacerbate the self-desiccation effect, thus increasing the autogenous shrinkage [91]. (2) the seeding effect of the nanomaterials can improve the hydration reaction so that the chemical shrinkage contributed to autogenous shrinkage [92].

Fig. 19 shows the isothermal calorimetry results. Fig. 19(a) shows the effect of nanoclay contents on the heat flow evolution of investigated UHPC mixtures. Fig. 19(b) shows the effect of nanoclay contents on the cumulative heat releases of investigated UHPC mixtures. As the nanoclay content increased from 0 to 0.20 %, the peak time of heat flow was advanced from 11.1 h to 10.1 h (by 9 %), and the cumulative heat release was increased from 64.3 J/g to 72.8 J/g (by 13 %). The results validated that the nanoclay addition can efficiently promote and accelerate the hydraulic reaction of investigated UHPC mixtures, which

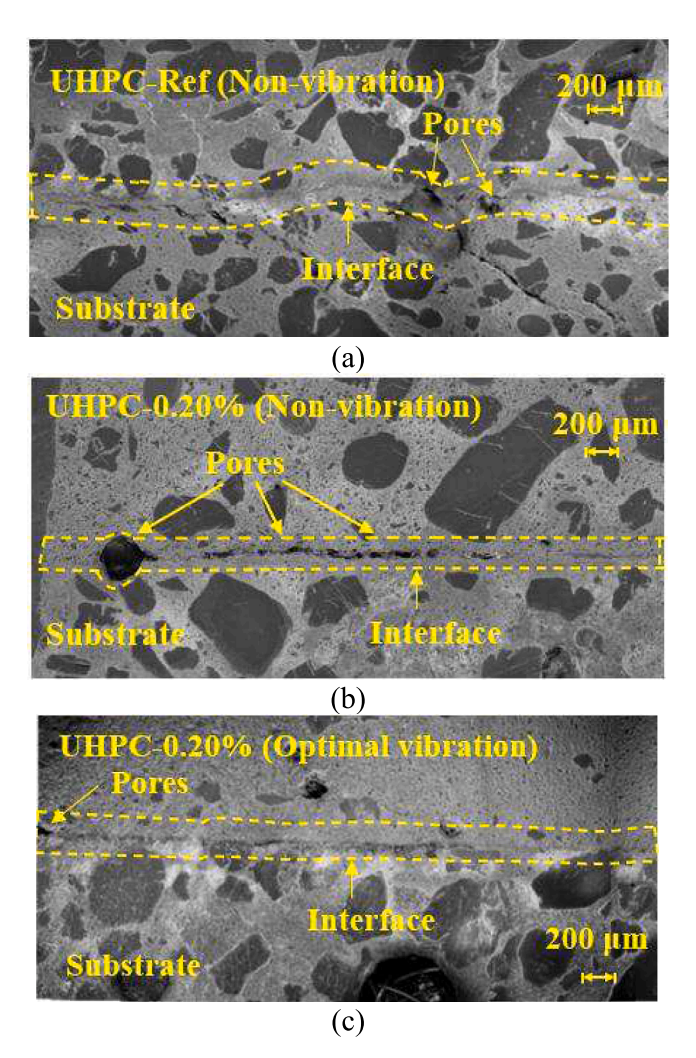


Fig. 23. The microstructures of the interface between substrate and UHPC overlay with different water-based nanoclay contents and vibrations: (a) UHPC-Ref (non-vibration); (b) UHPC-0.20% (non-vibration); and (c) UHPC-0.20% (optimal vibration).

validated the increasing of compressive strength and autogenous shrinkage.

# 4.1.5. Effect of nanoclay content on bond strength

Using the water-based nanoclay suspension, however, decreases the bond strength between the UHPC overlay and substrate. As shown in Fig. 20(a), as the water-based nanoclay contents increased from 0 to 0.20 %, the 3-day and 28-day bond strengths were reduced from 1.88 MPa to 1.25 MPa (by 34 %) and 2.33 MPa to 1.80 MPa (by 23 %), respectively. Fig. 20(b) showed that, under the external shear force, the failure was occurred at the interface between UHPC overlay and normal-strength mortar substrate in this research.

Due to the filler effect of nanoclay and microstructure refinement, the compressive strength of UHPC was improved with the adding of water-based nanoclay. However, the nanoclay could not refine the microstructure in the interfacial zone between the UHPC overlay and substrate. It is reasonable to speculate that the nanoclay particles in the UHPC could not fully contact with the substrate due to the following reason: (1) With the increasing of thixotropy by adding water-based nanoclay, the "intrusion capacity" of fresh UHPC is reduced, which prevents UHPC to fully contact with the surface of the substrate, leading to the formation of voids on the interface, as depicted in Fig. 20(c) and 20(d). (2) The air content is increased in UHPC due to the adding of nanoclay and voids on the interface. Thus, the bond strength of the interface was reduced. To validate this speculation, microstructural

analysis on the interface was discussed in Section 4.2.2.

# 4.2. Coupled effect of nanoclay and vibration on performance of UHPC as an overlay

As mentioned earlier, the high thixotropy of UHPC is beneficial for slope casting, because it prevents the free flow of fresh UHPC under gravity and facilitates the overlay construction. However, as discussed in 4.1.5, the improvement of thixotropy undermines the interfacial properties of overlay and substrate. To ensure the proper bond strength, vibration was applied and the coupled effect of nanoclay content and vibration on interfacial properties of UHPC overlay was investigated. Additionally, the applied vibration might break the reversible effect (i. e., physical particle flocculation) to partially restore the workability, which hinders the structural build-up of the thixotropic UHPC. Thus, the shape stability performance of thixotropic UHPC mixtures with waterbased nanoclay after the vibration was validated.

#### 4.2.1. Coupled effect of nanoclay and vibrations on bond strength

Haber et al. [17] revealed that the thixotropic material remains solid-like under static conditions but changes to flowable when suffering agitation and vibration. The vibration was proposed to improve the bond strength, because the vibration can release the entrapped air on the interface and the voids on the interface can be refilled by UHPC overlay. Fig. 21 shows the 3-day bond strength results after applying vibrations,

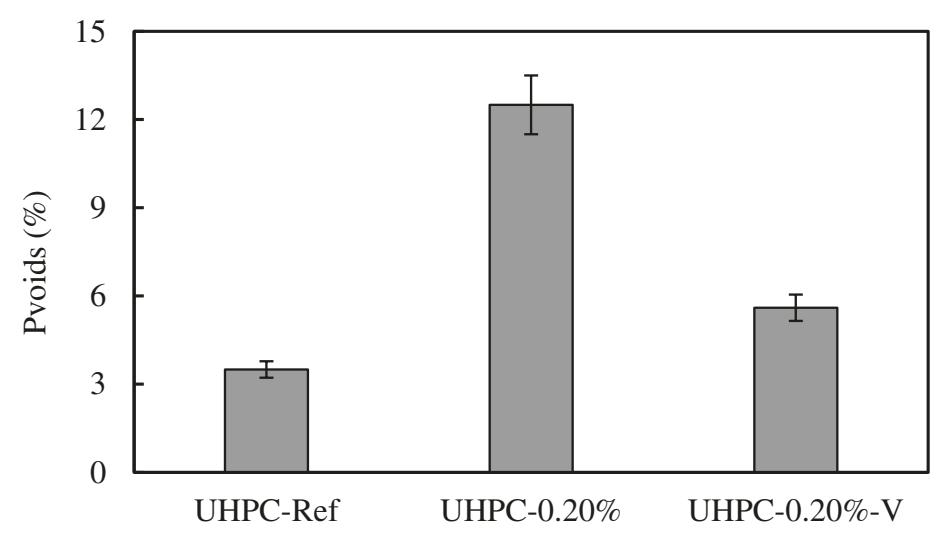


**Fig. 24.** The ratio ( $P_{voids}$ ) of interface length covered by air voids to the total length. Note: UHPC-0.20%-V represents the samples that were under optimal vibration. The data points in this figure are the average value of ten parallel experiments.

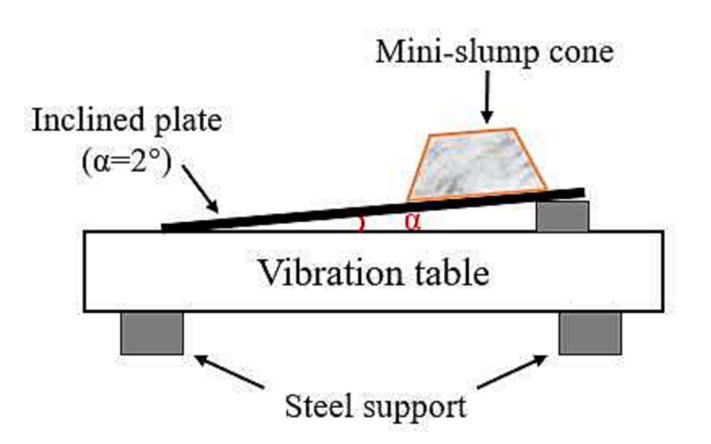


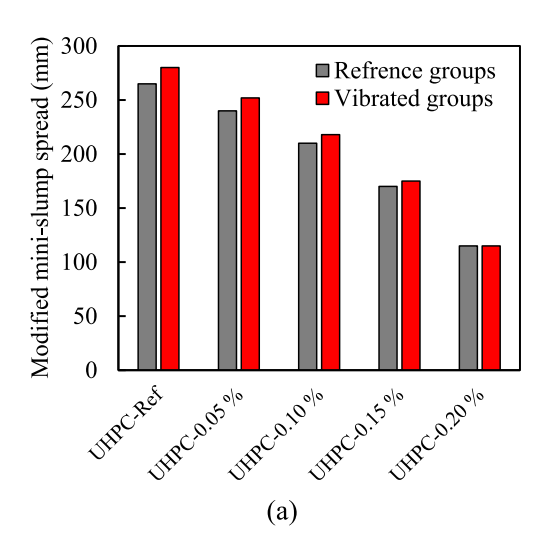
Fig. 25. The schematic diagram of the test set-up.

where the vibration amplitude was set as 0.79 mm and 1.58 mm, respectively. It can be seen that, as the vibration time increased, the bond strengths were first increased then stabilized. When the vibration

amplitude was set as 1.58 mm, the 3-day bond strengths were increased by 52 %, 53 %, 49 %, 70 %, and 80 % for UHPC-Ref, UHPC-0.05 %, UHPC-0.10 %, UHPC-0.1 %, and UHPC-0.20 %, and the vibration time for stabilization were 10 s, 15 s, 30 s, 45 s, and 45 s, respectively. The coefficients of the variance were approximately 8 %. When the vibration amplitude was set as 0.79 mm, the 3-day bond strengths were increased by 45 %, 45 %, 48 %, 62 %, and 80 % for UHPC-Ref, UHPC-0.05 %, UHPC-0.10 %, UHPC-0.15 %, and UHPC-0.20 %, and the vibration time for stabilization were 20 s, 30 s, 45 s, 60 s, and 60 s, respectively. The coefficient of variance were approximately 10 %. The results indicated that applying vibration can efficiently improve the bond strength. When the vibration amplitude is fixed, UHPC overlay with higher thixotropy requires longer vibration time to reach the optimal bond strength. And when the thixotropy of UHPC overlay is determined, applying higher vibration amplitude requires shorter vibration time to reach the optimal bond strength. In order to quantify the effect of the vibration, the vibration index (I<sub>v</sub>) is proposed, which is defined as the product of vibration amplitude and vibration time, as shown in Eq. (8):

$$E_V = A \times t \tag{8}$$

where  $I_V$  represents the vibration index, A represents the vibration



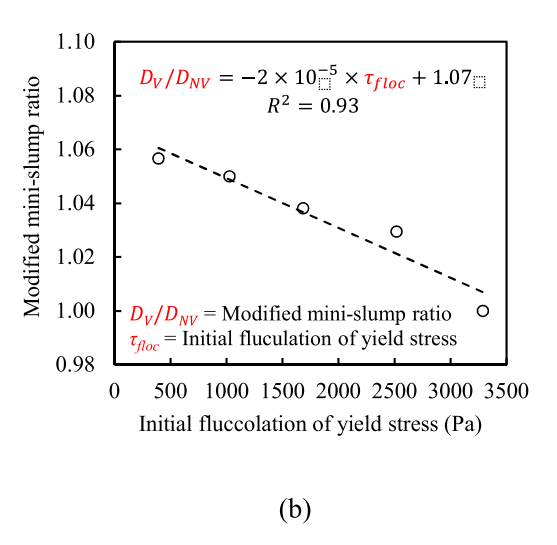


**Fig. 26.** The results of modified mini-slump test on the inclined plate: (a) modified mini-slump spreads of reference groups and vibrated groups; (b) the linear relationship between the modified mini-slump ratio  $(D_V/D_{NV})$  and initial fluctuation of yield stress  $(\tau_{floc})$ .

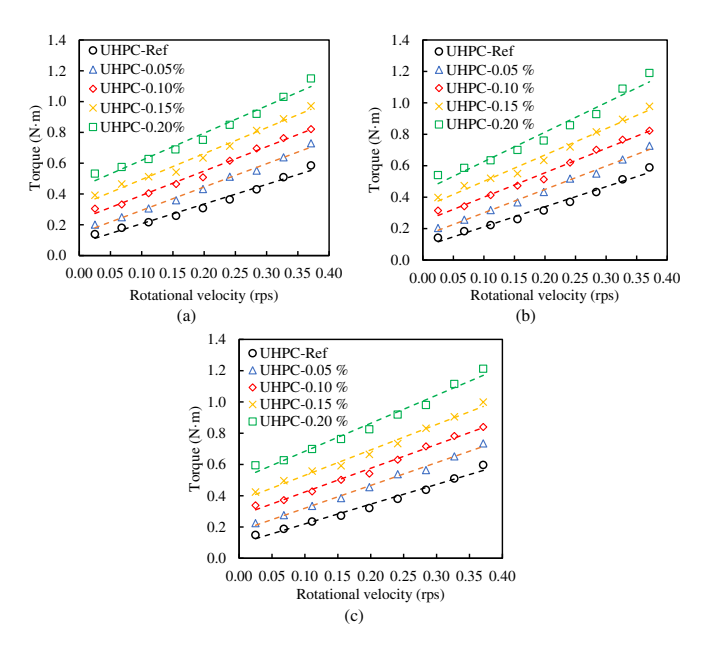


**Fig. A1.** Equilibrium flow curves of UHPC with different nanoclay contents at: (a) 6 min; (b) 16 min; and (c) 56 min.

amplitude, and t represents the vibration time.

Fig. 22(a) demonstrates the relationship between bond strength and vibration index  $(I_V)$ . The optimal vibration index is defined as the vibration index corresponding to the maximum bond strength. As the vibration index increased, the bond strengths were increased and then stabilized to a certain value. The optimal vibration index were determined to be 15.9 mm·s, 26.7 mm·s, 36.7 mm·s, 47.0 mm·s, and 53.9 mm·s for UHPC-Ref, UHPC-0.05 %, UHPC-0.10 %, UHPC-0.15 %, and UHPC-0.20 %, respectively. Fig. 22(b) shows the relationship between optimal vibration index and nanoclay suspension content through the regression analysis. The results indicated that the optimal vibration index is linearly increased with the increase of the water-based nanoclay contents or the thixotropic property of UHPC overlay. The results can be utilized as a guide to achieve satisfactory bond strength through the different combinations between vibration time and amplitude, given different types of vibrators. The underlying mechanism of improvement of bond strength by applying vibration index was discussed in Section 4.2.2.

# 4.2.2. Microstructural analysis of the interface before and after vibration

The interface quality between UHPC overlay and substrate was quantified by the SEM test. Specifically, according to [19], the ratio (i.e., the index  $P_{voids}$ ) of interface length covered by air voids to the total length of the interface was determined. The higher  $P_{voids}$  value represents a higher amount of voids on the interface. Fig. 23 shows the SEM images of the interface between UHPC overlay and substrate for different water-based nanoclay contents and vibration index. It was observed that unfilled voids on the interface were significantly increased with adding water-based nanoclay, but the voids were highly reduced when optimal vibration was applied.

Fig. 24 summarized the  $P_{voids}$  results of the interface between UHPC overlay and substrate with various nanoclay contents and vibration index levels. As the water-based nanoclay contents increased from 0 to 0.20 %, the  $P_{voids}$  increased from 3.5 % to 12.5 % (by 250 %). After the optimal vibration applied on the investigated samples, the  $P_{voids}$  was reduced from 12.0 % to 5.6 % (by 55 %). The results validated the speculation: the thixotropy of fresh UHPC can be improved by adding water-based nanoclay, which facilitates the overlay construction and improves the mechanical properties of UHPC by promoting its hydration. Although the interfacial properties between UHPC overlay and

substrate was compromised by introduced voids, the optimal vibration can be applied for thixotropic UHPC with a specific rheological property to minimize the voids on the interface based on optimal vibration index, thus achieving the highest bond strength.

# 4.2.3. Effect of vibration on shape stability of thixotropic UHPC with different nanoclay contents

Proper vibration is necessary to achieve satisfactory interfacial properties when highly thixotropic UHPC was used for overlay. However, the vibration can break the flocculation of particles to hinder the structural build-up of the thixotropic UHPC mixtures [93]. Therefore, the effect of the vibration on the shape stability of thixotropic UHPC with different water-based nanoclay contents was further discussed in this section.

To simulate the overlay on construction sites, an inclined plate with  $2^{\circ}$  slope was utilized [68], and the modified mini-slump test on the inclined plate was designed, as shown in Fig. 25. For reference groups (no vibration), after filling the UHPC, the mini-slump cone was held for 10 min on the inclined plate, and then lifted for the diameter measurement ( $D_{NV}$ ). For the vibrated groups, after filling the UHPC, the mini-slump cone was first held and vibrated (vibration time: 1 min; vibration amplitude: 0.79 mm), then further held for another 9 min, and finally lifted for the diameter measurement ( $D_V$ ). The ratio between  $D_V$  and  $D_{NV}$  was utilized to evaluate the shape stability of thixotropic UHPC mixtures.

Fig. 26(a) summarizes the results of modified mini-slump spreads. For the reference groups, the modified mini-slump spreads on the inclined plate were 265 mm, 240 mm, 210 mm, 170 mm, and 115 mm for UHPC-Ref, UHPC-0.05 %, UHPC-0.10 %, UHPC-0.15 %, and UHPC-0.20 %, respectively. For the vibrated groups, the modified mini-slump spreads on the inclined plate were 280 mm, 252 mm, 218 mm, 175 mm, and 115 mm for UHPC-Ref, UHPC-0.05 %, UHPC-0.10 %, UHPC-0.15 %, and UHPC-0.20 %, respectively. The corresponding modified mini-slump ratios ( $D_V/D_{NV}$ ) were 1.06, 1.05, 1.03, 1.02, and 1.00. The shape stability of UHPC mixtures can be better once  $D_V/D_{NV}$  is the closer to one. The results validated that, even if proper vibration was applied after placement, thixotropic UHPC mixtures with proper water-based nanoclay content showed good shape stability. In addition, the placement work was generally carried out immediately after the homogenization of UHPC mixtures, and the structural build-up of UHPC was mainly due to the physical particles flocculation. Based on that, a linear relationship between the modified mini-slump ratio  $(D_V/D_{NV})$  and initial fluctuation of yield stress ( $\tau_{floc}$ ) could be found by linear regression, as shown in Fig. 26(b).

# 5. Conclusion

A new type of water-based nanoclay suspension was used in this study to enhance thixotropy of UHPC mixtures. Firstly, the key properties and underlying mechanism of thixotropic UHPC itself with various nanoclay contents were investigated and elaborated. Subsequently, the coupled effects of nanoclay and vibration index on the interfacial properties between thixotropic UHPC overlay and substrate were revealed and analyzed. Based on the above investigations, the main findings can be summarized as follows:

- The addition of water-based nanoclay had negligible impacts on thixotropic UHPC production. As the nanoclay increased from 0 to 0.20 %, the peak mixing torque was increased by 3 % and the homogenization time was the same.
- The addition of water-based nanoclay effectively enhanced the thixotropy of UHPC. As the nanoclay increased from 0 to 0.20 %, the initial fluctuation of yield stress ( $\tau_{floc}$ ) was increased by 700 %, which mainly ascribed to the particles flocculation. Besides the thixotropy

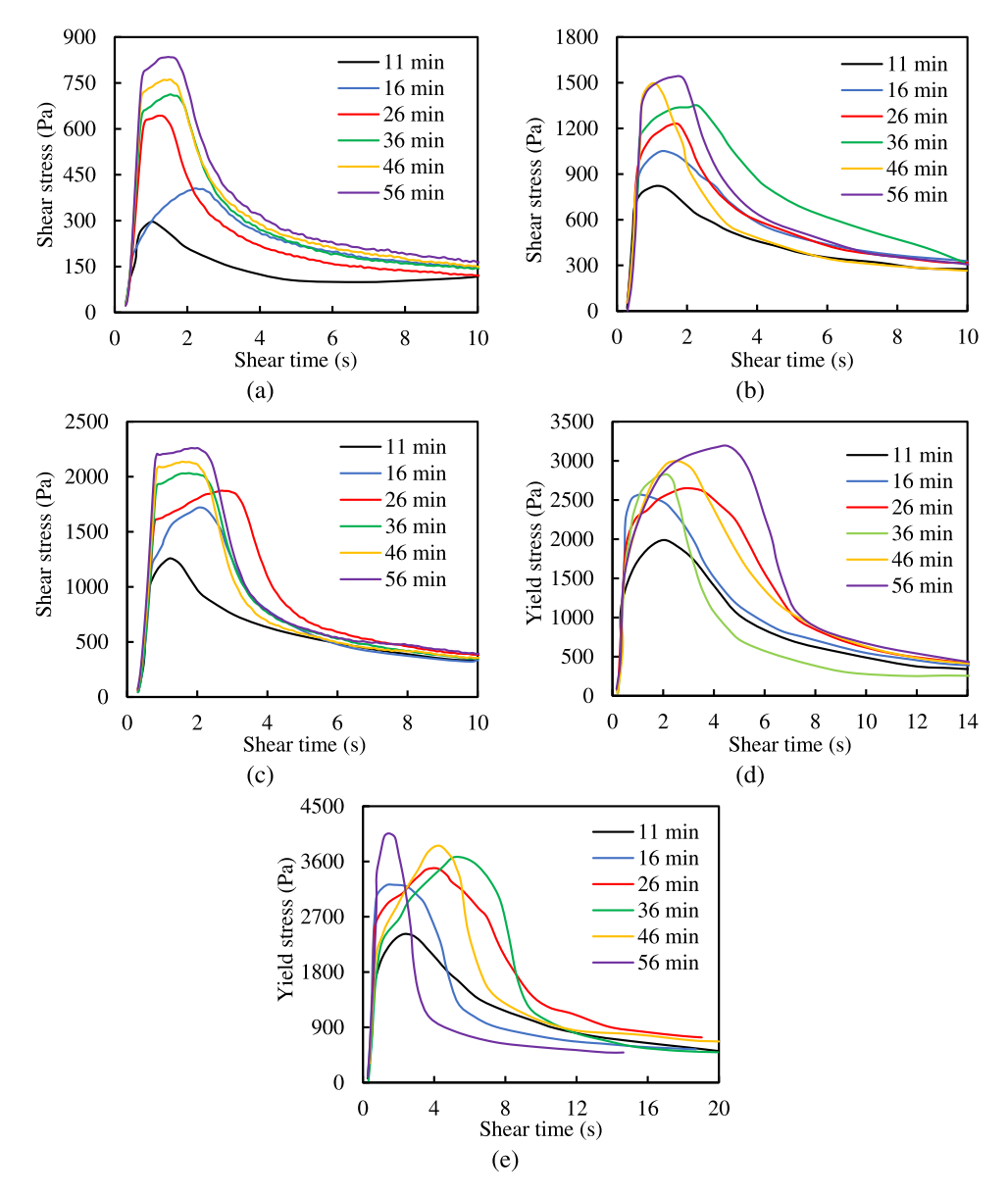


Fig. A2. The shear stress-shear time evolution curves: (a) UHPC-Ref; (b) UHPC-0.05%; (c) UHPC-0.10%; (d) UHPC-0.15%; and (e) UHPC-0.20%.

index  $(I_A)$  was increased by 70 %, which mainly ascribed to the improved hydration reaction.

- The addition of water-based nanoclay efficiently affected hardened properties of UHPC. As the nanoclay increased from 0 to 0.20 %, the 28-day compressive strength was increased by 7 % and the 28-day autogenous shrinkage was increased by 25 %.
- High thixotropy reduced the bond strength between UHPC overlay and substrate. However, proper vibration improved the bond strength without affecting the shape stability. As the nanoclay increased from 0 to 0.20 %, the 3-day bond strengths of UHPC-0.20 % were reduced by 34 % Applying the optimal vibration, the 3-day bond strength were increased by 80 % for UHPC-0.20 %.
- The underlying mechanism is applying appropriate vibration can temporarily restore the flowability of UHPC overlay and fill the voids on the interface, which improves the interfacial properties. As the nanoclay increased from 0 to 0.20 %, the *P*<sub>voids</sub> increased from 3.5 % to 12.5 %. However, by applying the optimal vibration, the *P*<sub>voids</sub> was reduced from 12.0 % to 5.6 %.

#### CRediT authorship contribution statement

**Jiang Du:** Data curation, Formal analysis, Investigation, Visualization, Writing – original draft. **Pengwei Guo:** Data curation, Investigation, Writing – review & editing. **Zhuo Liu:** Data curation, Validation, Writing – review & editing. **Weina Meng:** Conceptualization, Project administration, Resources, Supervision, Funding acquisition, Writing – review & editing.

# **Declaration of Competing Interest**

The authors declare that they have no known competing financial interests or personal relationships that could have appeared to influence the work reported in this paper.

# Data availability

Data will be made available on request.

#### Acknowledgement

This research is supported by the United States National Science Foundation [grant number: CMMI-2046407] and New Jersey Department of Transportation: Task Order 388 – Bridge Resource Program (2021-2022), contract ID number: 21-50862. The authors would like to thank Prof. Nassif and Dr. Abu-obeidah in Infrastructure Monitoring and Evaluation (RIME) Group from Rutgers for their support on this project. The authors also would like to thank Mr. Bill Kulish (the president of Steelike Inc) for the donation of steel fibers and ActiveMinerals for the donation of water-based nanoclay.

#### **Appendix**

#### References

- W. Meng, K.H. Khayat, Effects of saturated lightweight sand content on key characteristics of ultra-high-performance concrete, Cem. Concr. Res. 101 (2017) 46–54.
- [2] H. Huang, X. Gao, L. Teng, Fiber alignment and its effect on mechanical properties of UHPC: An overview, Constr. Build. Mater. 296 (2021), 123741.
- [3] Z. Lu, Z.-G. Feng, D. Yao, X. Li, H. Ji, Freeze-thaw resistance of Ultra-High performance concrete: Dependence on concrete composition, Constr. Build. Mater. 293 (2021), 123523.
- [4] J. Du, W. Meng, K.H. Khayat, Y. Bao, P. Guo, Z. Lyu, A. Abu-obeidah, H. Nassif, H. Wang, New development of ultra-high-performance concrete (UHPC), Engineering, Composites Part B, 2021, p. 109220.
- [5] J. Du, Z. Liu, C. Christodoulatos, M. Conway, Y. Bao, W. Meng, Utilization of off-specification fly ash in preparing ultra-high-performance concrete (UHPC): Mixture design, characterization, and life-cycle assessment, Resour. Conserv. Recycl. 180 (2022), 106136.
- [6] S. Mahjoubi, R. Barhemat, W. Meng, Y. Bao, AI-guided auto-discovery of lowcarbon cost-effective ultra-high performance concrete (UHPC), Resour. Conserv. Recycl. 189 (2023), 106741.
- [7] D. Fan, W. Tian, R. Yu, Incorporation of liquid phase into solid particle packing model for precise design of low water/binder cement-based composites (LW/B-CC): Modelling and experiments, Compos. B Eng. 242 (2022), 110070.
- [8] T. Alahmari, C. Kennedy, A. Cuaron, B. Weldon, D. Jauregui, Field testing of a prestressed concrete bridge with high performance and locally developed ultrahigh performance girders, Frontiers in Built Environment 5 (2019) 114.
- [9] Aaleti, S., Sritharan, S., and Abu-Hawash, A. Innovative UHPC-normal concrete composite bridge deck. in Proceedings of the RILEM-fib-AFGC International Symposium on Ultra-High Performance Reinforced Concrete, Eds: F. Toutlemonde, J. Resplendino, Rilem Publications SARL, Bagneux, France. 2013.
- [10] T.V. Voort, M.T. Suleiman, S. Sritharan, Design and performance verification of ultra-high performance concrete piles for deep foundations, Iowa State University. Center for Transportation Research and Education, 2008.
- [11] Y. Zou, K. Yu, J. Heng, Z. Zhang, H. Peng, C. Wu, X. Wang, Feasibility study of new GFRP grid web - Concrete composite beam, Compos. Struct. 305 (2023), 116527.
- [12] J. Qi, Y. Bao, J. Wang, L. Li, W. Li, Flexural behavior of an innovative dovetail UHPC joint in composite bridges under negative bending moment, Eng. Struct. 200 (2019), 109716.
- [13] Graybeal, B., Field-cast UHPC connections for modular bridge deck elements. 2010.
- [14] B.A. Graybeal, Ultra-high performance concrete composite connections for precast concrete bridge decks. United States, Federal Highway Administration, Office of Infrastructure Research and Development, 2012.
- [15] S. Verger-Leboeuf, J.-P. Charron, B. Massicotte, Design and behavior of UHPFRC field-cast transverse connections between precast bridge deck elements, J. Bridg. Eng. 22 (7) (2017) 04017031.
- [16] J. Xie, Q. Fu, J.-B. Yan, Compressive behaviour of stub concrete column strengthened with ultra-high performance concrete jacket, Constr. Build. Mater. 204 (2019) 643–658.
- [17] Haber, Z. B., Munoz, J. F., and Graybeal, B. A., Field testing of an ultra-high performance concrete overlay. 2017, United States. Federal Highway Administration. Office of Infrastructure.
- [18] Khayat, K. H. and Valipour, M., Design of ultra high performance concrete as an overlay in pavements and bridge decks. 2014, Missouri University of Science and Technology. Center for Transportation Infrastructure and Safety.
- [19] Z.B. Haber, J.F. Munoz, I. De la Varga, B.A. Graybeal, Bond characterization of UHPC overlays for concrete bridge decks: Laboratory and field testing, Constr. Build. Mater. 190 (2018) 1056–1068.
- [20] Wibowo, H. and Sritharan, S., Use of Ultra-High-Performance Concrete for Bridge Deck Overlays. 2018, United States. Federal Highway Administration.
- [21] L. Teng, M. Valipour, K.H. Khayat, Design and performance of low shrinkage UHPC for thin bonded bridge deck overlay, Cem. Concr. Compos. (2021), 103953.
- [22] Y. Zou, K. Zheng, Z. Zhou, Z. Zhang, J. Guo, J. Jiang, Experimental study on flexural behavior of hollow steel-UHPC composite bridge deck, Eng. Struct. 274 (2023), 115087.

- [23] K. Habel, E. Denarié, E. Brühwiler, Experimental investigation of composite ultrahigh-performance fiber-reinforced concrete and conventional concrete members, ACI Struct. J. 104 (1) (2007) 93.
- [24] Graybeal, B. A., Characterization of the behavior of ultra-high performance concrete (Doctoral dissertation). 2005.
- [25] A.A. Semendary, D. Svecova, Factors affecting bond between precast concrete and cast in place ultra high performance concrete (UHPC), Eng. Struct. 216 (2020), 110746.
- [26] M. Farzad, M. Shafieifar, A. Azizinamini, Experimental and numerical study on bond strength between conventional concrete and Ultra High-Performance Concrete (UHPC), Eng. Struct. 186 (2019) 297–305.
- [27] M. Berry, R. Snidarich, C. Wood, Development of Non-Proprietary Ultra-High Performance Concrete. Montana, Dept. of Transportation, Research Programs, 2017.
- [28] Q. Lu, J. Bors, Alternate uses of epoxy asphalt on bridge decks and roadways, Constr. Build. Mater. 78 (2015) 18–25.
- [29] S. Okba, A. El-Dieb, M. Reda, Evaluation of the corrosion resistance of latex modified concrete (LMC), Cem. Concr. Res. 27 (6) (1997) 861–868.
- [30] J. Xue, B. Briseghella, F. Huang, C. Nuti, H. Tabatabai, B. Chen, Review of ultrahigh performance concrete and its application in bridge engineering, Constr. Build. Mater. 260 (2020), 119844.
- [31] H. Peng, J. Yin, W. Song, Mechanical and hydraulic behaviors of eco-friendly pervious concrete incorporating fly ash and blast furnace slag, Appl. Sci. 8 (6) (2018) 859.
- [32] J. Silfwerbrand, H. Beushausen, Bonded concrete overlays—bond strength issues. in Proceedings ICCRRR, International Conference on Concrete Repair, Rehabilitation and Retrofitting, Cape Town, South Africa, Taylor & Francis Group, London, 2005, p. 2006.
- [33] D.P. Kumar, S. Amit, M.S.R. Chand, Influence of various nano-size materials on fresh and hardened state of fast setting high early strength concrete [FSHESC]: A state-of-the-art review, Constr. Build. Mater. 277 (2021), 122299.
- [34] J. Assaad, K.H. Khayat, H. Mesbah, Assessment of thixotropy of flowable and selfconsolidating concrete, Materials Journal 100 (2) (2003) 99–107.
- [35] G. De Schutter, K. Lesage, V. Mechtcherine, V.N. Nerella, G. Habert, I. Agusti-Juan, Vision of 3D printing with concrete — Technical, economic and environmental potentials, Cem. Concr. Res. 112 (2018) 25–36.
- [36] O.A.M. Reales, P. Duda, E.C. Silva, M.D. Paiva, R.D. Toledo Filho, Nanosilica particles as structural buildup agents for 3D printing with Portland cement pastes, Constr. Build. Mater. 219 (2019) 91–100.
- [37] J. Kruger, S. Zeranka, G. van Zijl, 3D concrete printing: a lower bound analytical model for buildability performance quantification, Autom. Constr. 106 (2019), 102904.
- [38] Y. Cai, Q.-F. Liu, L. Yu, Z. Meng, Z. Hu, Q. Yuan, B. Šavija, An experimental and numerical investigation of coarse aggregate settlement in fresh concrete under vibration, Cem. Concr. Compos. 122 (2021), 104153.
- [39] L. Teng, W. Meng, K.H. Khayat, Rheology control of ultra-high-performance concrete made with different fiber contents, Cem. Concr. Res. 138 (2020), 106222.
- [40] W. Meng, K.H. Khayat, Improving flexural performance of ultra-high-performance concrete by rheology control of suspending mortar, Compos. B Eng. 117 (2017) 26–34.
- [41] K.H. Khayat, W. Meng, K. Vallurupalli, L. Teng, Rheological properties of ultrahigh-performance concrete—An overview, Cem. Concr. Res. 124 (2019), 105828.
- [42] D. Jiao, R. De Schryver, C. Shi, G. De Schutter, Thixotropic structural build-up of cement-based materials: A state-of-the-art review, Cem. Concr. Compos. (2021), 104152
- [43] S. Kawashima, K. Wang, R.D. Ferron, J.H. Kim, N. Tregger, S. Shah, A review of the effect of nanoclays on the fresh and hardened properties of cement-based materials, Cem. Concr. Res. 147 (2021), 106502.
- [44] L. Teng, J. Zhu, K.H. Khayat, J. Liu, Effect of welan gum and nanoclay on thixotropy of UHPC, Cem. Concr. Res. 138 (2020), 106238.
- [45] S. Ma, Y. Qian, S. Kawashima, Experimental and modeling study on the non-linear structural build-up of fresh cement pastes incorporating viscosity modifying admixtures, Cem. Concr. Res. 108 (2018) 1–9.
- [46] L. Keke, L. Yong, X. Liuliu, Z. Junjie, L. Kangning, F. Dingqiang, Y. Rui, Rheological characteristics of Ultra-High performance concrete (UHPC) incorporating bentonite, Constr. Build. Mater. 349 (2022), 128793.
- [47] S. Kawashima, J.H. Kim, D.J. Corr, S.P. Shah, Study of the mechanisms underlying the fresh-state response of cementitious materials modified with nanoclays, Constr. Build. Mater. 36 (2012) 749–757.
- [48] S. Ma, S. Kawashima, A rheological approach to study the early-age hydration of oil well cement: Effect of temperature, pressure and nanoclay, Constr. Build. Mater. 215 (2019) 119–127.
- [49] Y. Qian, G. De Schutter, Enhancing thixotropy of fresh cement pastes with nanoclay in presence of polycarboxylate ether superplasticizer (PCE), Cem. Concr. Res. 111 (2018) 15–22.
- [50] Z. Liu, J. Du, W. Meng, Achieving low-carbon cementitious materials with high mechanical properties using CaCO3 suspension produced by CO2 sequestration, J. Clean. Prod. 373 (2022), 133546.
- [51] Qian, Y., Characterization of structural rebuilding and shear migration in cementitious materials in consideration of thixotropy (Doctoral dissertation). 2017.
- [52] Q. Yuan, D. Zhou, B. Li, H. Huang, C. Shi, Effect of mineral admixtures on the structural build-up of cement paste, Constr. Build. Mater. 160 (2018) 117–126.
- [53] Y. Qian, S. Kawashima, Use of creep recovery protocol to measure static yield stress and structural rebuilding of fresh cement pastes, Cem. Concr. Res. 90 (2016) 73–79.

- [54] R.D. Ferron, S. Shah, E. Fuente, C. Negro, Aggregation and breakage kinetics of fresh cement paste, Cem. Concr. Res. 50 (2013) 1–10.
- [55] H. Varela, G. Barluenga, I. Palomar, Influence of nanoclays on flowability and rheology of SCC pastes, Constr. Build. Mater. 243 (2020), 118285.
- [56] W. Meng, K.H. Khayat, Effect of graphite nanoplatelets and carbon nanofibers on rheology, hydration, shrinkage, mechanical properties, and microstructure of UHPC, Cem. Concr. Res. 105 (2018) 64–71.
- [57] M.S. Konsta-Gdoutos, Z.S. Metaxa, S.P. Shah, Highly dispersed carbon nanotube reinforced cement based materials, Cem. Concr. Res. 40 (7) (2010) 1052–1059.
- [58] A. Peyvandi, P. Soroushian, N. Abdol, A.M. Balachandra, Surface-modified graphite nanomaterials for improved reinforcement efficiency in cementitious paste, Carbon 63 (2013) 175–186.
- [59] H. Wu, K. Huang, W. Song, F. He, Characterizing the fatigue cracking behaviors of OGFC pavements using the overlay tester, Constr. Build. Mater. 307 (2021), 124979
- [60] W. Song, Z. Xu, F. Xu, H. Wu, J. Yin, Fracture investigation of asphalt mixtures containing reclaimed asphalt pavement using an equivalent energy approach, Eng. Fract. Mech. 253 (2021), 107892.
- [61] J. Yang, J. Xia, Z. Zhang, Y. Zou, Z. Wang, J. Zhou, Experimental and numerical investigations on the mechanical behavior of reinforced concrete arches strengthened with UHPC subjected to asymmetric load. Structures, Elsevier, 2022.
- [62] A. Valikhani, A.J. Jahromi, I.M. Mantawy, A. Azizinamini, Experimental evaluation of concrete-to-UHPC bond strength with correlation to surface roughness for repair application, Constr. Build. Mater. 238 (2020), 117753.
- [63] Y. Zhang, P. Zhu, Z. Liao, L. Wang, Interfacial bond properties between normal strength concrete substrate and ultra-high performance concrete as a repair material, Constr. Build. Mater. 235 (2020), 117431.
- [64] L. Teng, K.H. Khayat, Effect of overlay thickness, fiber volume, and shrinkage mitigation on flexural behavior of thin bonded ultra-high-performance concrete overlay slab, Cem. Concr. Compos. 134 (2022), 104752.
- [65] Y. Zhang, C. Zhang, Y. Zhu, J. Cao, X. Shao, An experimental study: various influence factors affecting interfacial shear performance of UHPC-NSC, Constr. Build. Mater. 236 (2020), 117480.
- [66] Z. Wu, K.H. Khayat, C. Shi, Changes in rheology and mechanical properties of ultrahigh performance concrete with silica fume content, Cem. Concr. Res. 123 (2019), 105786
- [67] Q. Yuan, D. Zhou, K.H. Khayat, D. Feys, C. Shi, On the measurement of evolution of structural build-up of cement paste with time by static yield stress test vs. small amplitude oscillatory shear test, Cem. Concr. Res. 99 (2017) 183–189.
- [68] K.H. Khayat, A.F. Omran, S. Naji, P. Billberg, A. Yahia, Field-oriented test methods to evaluate structural build-up at rest of flowable mortar and concrete, Mater. Struct. 45 (10) (2012) 1547–1564.
- [69] A.M. Mostafa, A. Yahia, New approach to assess build-up of cement-based suspensions. Cem. Concr. Res. 85 (2016) 174–182.
- [70] N. Roussel, Steady and transient flow behaviour of fresh cement pastes, Cem. Concr. Res. 35 (9) (2005) 1656–1664.
- [71] ASTM C1437-20, Standard Test Method for Flow of Hydraulic Cement Mortar. 2020.
- [72] J. Kruger, S. Zeranka, G. van Zijl, An ab initio approach for thixotropy characterisation of (nanoparticle-infused) 3D printable concrete, Constr. Build. Mater. 224 (2019) 372–386.
- [73] Q. Yuan, Z. Li, D. Zhou, T. Huang, H. Huang, D. Jiao, C. Shi, A feasible method for measuring the buildability of fresh 3D printing mortar, Constr. Build. Mater. 227 (2019), 116600.

- [74] Standard Specification for Compressive Strength of Hydraulic Cement Mortars (Using 50 mm Cube Specimens). 2020, ASTM International.
- [75] R. Yang, R. Yu, Z. Shui, X. Gao, X. Xiao, X. Zhang, Y. Wang, Y. He, Low carbon design of an ultra-high performance concrete (UHPC) incorporating phosphorous slag, J. Clean. Prod. 240 (2019), 118157.
- [76] A. Momayez, M. Ehsani, A. Ramezanianpour, H. Rajaie, Comparison of methods for evaluating bond strength between concrete substrate and repair materials, Cem. Concr. Res. 35 (4) (2005) 748–757.
- [77] S.M. Iveson, P.A. Wauters, S. Forrest, J.D. Litster, G.M. Meesters, B. Scarlett, Growth regime map for liquid-bound granules: further development and experimental validation, Powder Technol. 117 (1–2) (2001) 83–97.
- [78] S.M. Iveson, J.D. Litster, K. Hapgood, B.J. Ennis, Nucleation, growth and breakage phenomena in agitated wet granulation processes: a review, Powder Technol. 117 (1–2) (2001) 3–39.
- [79] Billberg, P., Form pressure generated by self-compacting concrete: influence of thixotropy and structural behaviour at rest (Doctoral dissertation). 2006.
- [80] G.H. Tattersall, and Banfill, The rheology of fresh concrete, P. F., 1983.
- [81] S. Kawashima, P. Hou, D.J. Corr, S.P. Shah, Modification of cement-based materials with nanoparticles, Cem. Concr. Compos. 36 (2013) 8–15.
- [82] X. Zhang, H. Sun, H. Yang, R. Mu, H. Chen, Rheological properties of nanosilicamodified cement paste at different temperatures and hydration times, J. Mater. Civ. Eng. 33 (1) (2021) 04020404.
- [83] A. Quennoz, K.L. Scrivener, Interactions between alite and C3A-gypsum hydrations in model cements, Cem. Concr. Res. 44 (2013) 46–54.
- [84] D. Kong, S. Huang, D. Corr, Y. Yang, S.P. Shah, Whether do nano-particles act as nucleation sites for CSH gel growth during cement hydration? Cem. Concr. Compos. 87 (2018) 98–109.
- [85] G.H. Tattersall, Workability and quality control of concrete, CRC Press, 1991.
- [86] P. Guo, J. Du, Y. Bao, W. Meng, Real-time video recognition for assessing plastic viscosity of ultra-high-performance concrete (UHPC), Measurement 191 (2022), 110809
- [87] C. Jakob, D. Jansen, N. Ukrainczyk, E. Koenders, U. Pott, D. Stephan, J. Neubauer, Relating ettringite formation and rheological changes during the initial cement hydration: a comparative study applying XRD analysis, rheological measurements and modeling, Materials 12 (18) (2019) 2957.
- [88] N. Roussel, H. Bessaies-Bey, S. Kawashima, D. Marchon, K. Vasilic, R. Wolfs, Recent advances on yield stress and elasticity of fresh cement-based materials, Cem. Concr. Res. 124 (2019), 105798.
- [89] W. Song, J. Yi, H. Wu, X. He, Q. Song, J. Yin, Effect of carbon fiber on mechanical properties and dimensional stability of concrete incorporated with granulated-blast furnace slag, J. Clean. Prod. 238 (2019), 117819.
- [90] H. Huang, T. Huang, Q. Yuan, D. Zhou, D. Deng, L. Zhang, Temperature dependence of structural build-up and its relation with hydration kinetics of cement pasts. Constr. Build. Mater. 201 (2019) 553–562.
- [91] W. Meng, K.H. Khayat, Mechanical properties of ultra-high-performance concrete enhanced with graphite nanoplatelets and carbon nanofibers, Compos. B Eng. 107 (2016) 113–122.
- [92] D.-Y. Yoo, T. Oh, N. Banthia, Nanomaterials in ultra-high-performance concrete (UHPC)—A review, Cem. Concr. Compos. (2022), 104730.
- [93] Y.A. Abebe, L. Lohaus, Rheological characterization of the structural breakdown process to analyze the stability of flowable mortars under vibration, Constr. Build. Mater. 131 (2017) 517–525.